



HAL
open science

U–Pb detrital zircon geochronology and source provenance in the Moroccan Meseta (Variscan belt): A perspective from the Rehamna massif

Mehdi Jouhari, Francis Chopin, Mohamed El Houicha, Jean-François Ghienne, Karel Schulmann, Jitka Míková, Michel Corsini

► To cite this version:

Mehdi Jouhari, Francis Chopin, Mohamed El Houicha, Jean-François Ghienne, Karel Schulmann, et al.. U–Pb detrital zircon geochronology and source provenance in the Moroccan Meseta (Variscan belt): A perspective from the Rehamna massif. *Journal of African Earth Sciences*, 2022, 194, pp.104610. 10.1016/j.jafrearsci.2022.104610 . hal-03841054

HAL Id: hal-03841054

<https://hal.science/hal-03841054>

Submitted on 6 Nov 2022

HAL is a multi-disciplinary open access archive for the deposit and dissemination of scientific research documents, whether they are published or not. The documents may come from teaching and research institutions in France or abroad, or from public or private research centers.

L'archive ouverte pluridisciplinaire **HAL**, est destinée au dépôt et à la diffusion de documents scientifiques de niveau recherche, publiés ou non, émanant des établissements d'enseignement et de recherche français ou étrangers, des laboratoires publics ou privés.

1 **U–Pb detrital zircon geochronology and source provenance in the Moroccan Meseta**
2 **(Variscan belt): a perspective from the Rehamna massif**

3 Mehdi JOUHARI^{1,2}, Francis CHOPIN^{1,2*}, Mohamed EL HOUICHA³, Jean-François
4 GHIENNE¹, Karel SCHULMANN^{1,2}, Jitka MÍKOVÁ⁴, Michel CORSINI⁵

5
6 ¹ Institut Terre et Environnement de Strasbourg, UMR 7063, Université de Strasbourg, CNRS
7 – France

8 ² Centre for Lithospheric Research, Czech Geological Survey – Czech Republic

9 ³ LGG, Faculté des Sciences, Université Chouaïb Doukkali, El Jadida – Morocco

10 ⁴ Laboratories of the Czech Geological Survey, Prague – Czech Republic

11 ⁵ Géoazur UMR 6526, Université Côte d'Azur – France

12 *Corresponding author: Francis Chopin

13 **Keywords**

14 Detrital zircon geochronology, Rehamna, Moroccan Variscan belt, Paleozoic

15 **Abstract**

16 Metasandstones from early Cambrian to early Carboniferous stratigraphic successions were
17 sampled in the Rehamna massif of the Western Meseta in Morocco. The early Cambrian sample
18 shows a single Paleoproterozoic population at ca. 2 Ga suggesting a local basement source. The
19 Ordovician sample is largely dominated by a Cryogenian-Ediacaran population and minor
20 Paleoproterozoic peaks. The Devonian sample reveals age populations similar to North-West
21 African Cambrian to Devonian age spectra indicating that the southern-derived West
22 Gondwana source essentially pertained up to the Devonian. The two early Carboniferous
23 samples show more heterogeneous zircon age spectra with a marked Ediacaran peak

24 accompanied by Paleoproterozoic and Mesoproterozoic sub-peaks indicating important re-
25 organization of the drainage systems. One sample also shows presence of Upper Devonian to
26 early Carboniferous zircon grains, which suggests local magmatic sources associated to the
27 formation of intracontinental extensional basins. The comparison of detrital zircon spectra with
28 paleogeographic reconstructions indicate that the early Carboniferous change in detrital zircon
29 sources can be interpreted in the framework of the opening of the Paleotethys ocean with coeval
30 erosion of orogenic topographies linked to the emplacement of a Mid-Variscan Allochthon,
31 and/or collision of an Avalonian indenter to the north.

32 **Introduction**

33 This paper presents a detrital zircon U–Pb geochronology study of samples from the Rehamna
34 massif in the Moroccan Variscan belt (Michard *et al.*, 2010), which aims at better constraining
35 its lithostratigraphy and the evolution of source provenance during the Lower Paleozoic
36 development. The hardness and resistance to chemical weathering make zircon one of the most
37 durable minerals. Therefore, it can survive wide range of geological process (e.g.
38 metamorphism, erosion and sedimentary transport) and preserve primary source signatures
39 (Hanchar *and* Miller, 1993). In particular, detrital zircon grains in sedimentary rocks can
40 survive multiple sedimentary cycles involving the recycling of old sedimentary, igneous and
41 metamorphic rocks and younger primary crystalline sources (Thomas, 2011). Age distribution
42 of detrital zircon in sedimentary rocks can be used for correlation of similar stratigraphic units,
43 provenance analysis via comparison with known sources and determination of maximum
44 depositional ages in the absence of datable contemporaneous volcanic rocks (Reiners *et al.*,
45 2017).

46 The paleogeographic evolution of the Moroccan Variscan belt (Fig. 1) is mostly based on
47 geological mapping, tectonic studies and lithological correlations (Hoepffner *et al.*, 2005;
48 Simancas *et al.*, 2005, 2009; Michard *et al.*, 2010; Chopin *et al.*, 2014). These ideas were

49 recently tested by a new generation of detrital zircon studies mostly used to precise
50 paleogeography and source areas in northern Gondwana (e.g. Pereira *et al.*, 2014; Perez-Caseres
51 *et al.*, 2017; Letsch *et al.*, 2017; El Houicha *et al.*, 2018; Ghienne *et al.*, 2018; Perez *et al.*,
52 2019; Accotto *et al.*, 2019, 2020, 2021a,b, 2022 and references therein). So far examined
53 detrital zircon populations concern sedimentary rocks deposited in various late Neoproterozoic
54 to Paleozoic basins preserved in the Moroccan Meseta. Their origin generally refers to recycling
55 of the West African Craton (Archean domains, Eburnean Orogeny), the Pan-African Trans-
56 Saharan belt, the Saharan Metacraton to the east, and their overlying Paleozoic strata (e.g.,
57 Accotto *et al.*, 2019). Some studies focused on complete stratigraphic sections allow evaluating
58 evolution of source areas through time or possible impact of remote geodynamic processes (e.g.
59 Gärtner *et al.*, 2017; Accotto *et al.*, 2021). In this context, the Rehamna massif still remains
60 understudied.

61 To fill the gap, a detrital zircon U–Pb geochronology study of a deformed Paleozoic
62 sequence was performed in the southern part of the Rehamna massif of the Moroccan Meseta
63 (Fig. 1). The present study aims at determining maximum depositional age of the strata and to
64 give new insights into sedimentary provenance in an area where structural and stratigraphic
65 uncertainties persist to date. Finally, this study allows to contribute to better understand the
66 tectonic evolution of the northern Gondwana during late Paleozoic times.

67 **Geological setting**

68 The Paleozoic evolution of the Moroccan Variscan belt (Fig. 1) is well integrated in the
69 evolution of the northern margin of Gondwana from its early Paleozoic extensional basins until
70 its amalgamation with Laurussia during the late Carboniferous-early Permian (Michard *et al.*,
71 2010; Chopin *et al.*, 2014; Martínez Catalán *et al.*, 2021). Three main Paleozoic events can be
72 distinguished: (1) Since the late Cambrian formation of the Rheic ocean, the northern edge of
73 the West African Craton (WAC) evolved in a passive margin environment (Stampfli *and* Borel,

74 2002; Ribeiro *et al.*, 2007; Oriolo *et al.*, 2021). Avigad *et al.*, (2012) showed that until the late
75 Devonian, the sedimentation reflects the decreasing contribution of detrital material derived
76 from local sources. (2) Subsequent formation of the Paleotethys ocean was associated to late
77 Devonian-early Carboniferous intracontinental rifting (Stampfli *and* Borel, 2002; Frizon de
78 Lamotte *et al.*, 2013). (3) This event was followed by the late Carboniferous-early Permian
79 intracontinental Variscan Orogeny triggered by the collision between Gondwana with the
80 European Variscan belt and Laurussia, which ultimately lead to the formation of Pangea
81 (Hoepffner *et al.*, 2005; Michard *et al.*, 2010; Chopin *et al.*, 2014).

82 The Moroccan Meseta shows rare Precambrian basement units (e.g. Pereira *et al.*, 2015;
83 El Houicha *et al.*, 2018) unconformably overlain by thick Paleozoic successions deformed
84 during the late Paleozoic (Michard *et al.*, 2010; Chopin *et al.*, 2014). The Variscan belt in
85 Morocco can be divided into two main tectonic domains (Fig. 1; e.g., Piqué *et al.*, 1993a;
86 Hoepffner *et al.*, 2005; Michard *et al.*, 2010): (1) the southern thick-skinned Anti-Atlas belt
87 showing a fold and thrust belt with Paleozoic cover variably detached from its Precambrian
88 basement, and (2) the Moroccan Meseta domain to the north of the Southern Meseta Fault
89 (SMF) subdivided into two main zones, the Eastern and Western Meseta. The Eastern Meseta
90 (e.g. Middelt, Tazekka, Debdou-Mekkam massifs) is characterized by deformed pre-
91 Carboniferous sediments unconformably overlain by middle Visian to Serpukhovian-
92 Bashkirian deposits (Hoepffner, 1987; Accotto *et al.*, 2019, 2020). The Western Meseta
93 (Michard *et al.*, 2010) consists of almost undeformed Cambrian-Devonian strata of its western
94 “Coastal Block” and a central highly deformed and metamorphosed zone composed of
95 crystalline basement covered by Cambrian-Carboniferous strata (Chopin *et al.*, 2014; Delchini
96 *et al.*, 2018) outcropping in the Western High Atlas, Jebilet, Rehamna and Central massifs. The
97 exotic Sehoul Block is located to the northwest and is either assumed to have an Avalonia (El
98 Hassani, 1991; Piqué *et al.*, 1993b; Tahiri *et al.*, 2010) or Meguma affinity (Michard *et al.*,

99 2010) and was accreted to the Moroccan Meseta during the early Carboniferous (Tahiri *et al.*,
100 2010).

101 **Geology of the Rehamna massif**

102 The Paleozoic Rehamna massif is situated midway south of Casablanca and north of Marrakech
103 in the Western Meseta (Fig. 1). Its southern part is sometimes called the Rehamna metamorphic
104 dome in contrast to the northern part (not shown in Fig. 2), which reveals solely the presence
105 of comprehensive Cambrian to Permian sedimentary sequences. In this work we deal
106 exclusively with the metamorphic southern part, which is also characterized by Precambrian
107 inliers. The Rehamna massif is traditionally divided into three Western, Central and Eastern
108 Rehamna zones separated by the Western Meseta Shear Zone (WMSZ, Fig. 1) or Median Fault
109 and the Ouled Zednes Fault (Fig. 2; Michard *et al.*, 2010; Chopin *et al.*, 2014). Based on the
110 intensity of deformation and the degree of metamorphism, the southern part is further
111 subdivided into upper and lower metamorphic units (Fig. 3) according to the intensity of
112 deformation and the degree of metamorphism (Baudin *et al.*, 2003; Razin *et al.*, 2003; Michard
113 *et al.*, 2010; Chopin *et al.*, 2014).

114 **Lithostratigraphy**

115 In contrast to the northern part of the Rehamna massif, where the age of the temporal framework
116 of the succession is well understood (e.g. Hollard *et al.*, 1982; El Kamel, 2002), the
117 lithostratigraphy of its southern part is still controversial (Fig. 3; Destombes *et al.*, 1982; Baudin
118 *et al.*, 2003; Razin *et al.*, 2003; Michard *et al.*, 2010). In the lower metamorphic units of the
119 Central and Eastern Rehamna, the amphibolite facies metamorphism obliterated fossiliferous
120 records, and the tentative stratigraphy is solely based on facies analogies with fossiliferous
121 sedimentary sequences cropping out to the north (Hoepffner, 1974; Jenny, 1974).

122 The Paleoproterozoic basement of the Western Rehamna is characterized by
123 metamorphosed porphyroids and rhyolites (Pereira *et al.*, 2015) covered by low-grade early-

124 middle Cambrian sediments (Fig. 3; Corsini *et al.*, 1988). The sequence starts with early
125 Cambrian arkoses and limestones showing a gradually increasing detrital component (e.g. Lalla
126 Mouchaa Formation; El Houicha *et al.*, 2018). This formation is conformably overlain by the
127 “Paradoxides Shale Formation” composed of siltstone, greywacke and sandstone preserving a
128 middle Cambrian fauna (Guézou *and* Michard, 1976; Corsini *et al.*, 1988).

129 To the east of the WMSZ₇, a similar succession is present in the lower metamorphic unit
130 of the Central Rehamna. Here, an early Ediacaran (593±8 Ma; Baudin *et al.*, 2003) rhyolitic
131 basement crops out in the core of the Sidi Ali dome (Fig.2; Corsini *et al.*, 1988) and is
132 conformably overlain by early Cambrian terrigenous clastic sediments (conglomerate,
133 displaying granite and quartzite pebbles, interbedded with arkosic sandstone and mudstone;
134 Fig. 3). A limestone sequence (including calcschists interbeds) marks the transition to early
135 Cambrian siliciclastic sedimentation (Corsini *et al.*, 1988). The succession continues with early-
136 middle Cambrian metapelitic strata (Draa El Kebir Formation) unconformably overlain by the
137 Kef El Mouneb metaconglomerate assumingly Devonian (e.g. Hoepffner *et al.*, 1972). The age
138 of the quartzites from the Skhour Formation of the upper metamorphic allochthonous unit is
139 still controversial and was considered to be Ordovician by Destombes *et al.* (1982). However,
140 based on structural and sedimentological arguments, Baudin *et al.* (2003) and Michard *et al.*
141 (2010) alternatively proposed a possible Upper Devonian age for this formation (Fig. 3). The
142 structurally lower metamorphic unit of the Eastern Rehamna is divided into the Devonian
143 (Ouled Hassine-Ouled Zednes, OH-OZ) and Carboniferous (Lalla Tittaf) formations (Fig. 3).
144 The former formation corresponds to a succession of pelitic beds interbedded with poorly-
145 preserved Crinoidea-bearing limestones (Baudin *et al.*, 2003) and limy/sandy conglomerates or
146 quartzites, generally attributed to the Devonian (Hoepffner, 1974). Preserved Eifelian-Frasnian
147 corals were recently reported from this formation (marble of the Ouled Zednes area; El Houicha
148 *et al.*, 2019). The Lala Tittaf Formation consists of pelites intercalated with andesites, gabbros

149 and rhyolites (Hoepffner, 1974; Cornée, 1982). Considered first as Carboniferous, Baudin *et al.*
150 (2003) proposed a Paleoproterozoic age based on the dating of zircon grains from a gabbroic
151 intrusion (2136 ± 17 Ma). However, this was challenged by a new U–Pb zircon data which
152 provide early Carboniferous ages (339.5 ± 0.89 Ma) for the intraformational rhyolite sills (Aït
153 Lahna *et al.*, 2018).

154 The upper unit to the north is formed by the allochthonous and very low grade Jbel
155 Kharrou and Koudiat El Adam Formations (Fig. 2) which are made of Middle Ordovician to
156 Silurian shale and sandstone (Destombes *et al.*, 1982). To the southeast and south of the Ouled
157 Ouggad Fault, the upper unit is represented by various virtually unmetamorphosed rocks (Fig.
158 2). The latter are composed of Ordovician strata overlain by Devonian (-Tournaisian?)
159 sandstone and pelite and by the middle (?) late Viséan to Serpukhovian sandstone and limestone
160 including a sandy flysch facies typifying in the Dalaat unit (Fig. 3; Cornée, 1982; Razin *et al.*,
161 2003).

162 **Magmatism and metamorphism**

163 Two main metamorphic events were described in the southern part of the Rehamna massif. The
164 first one corresponds to a prograde Barrovian metamorphism (D1-M1) reaching the staurolite
165 (kyanite) stability field with estimated peak P-T at conditions 6–9 kbar and 410–560 °C. This
166 metamorphism affects the lower metamorphic unit during the late Carboniferous-early Permian
167 and was interpreted as a result of tectonic burial (Hoepffner *et al.*, 1982; Aghzer and Arenas,
168 1995; El Mahi *et al.*, 1999; Chopin *et al.*, 2014; Wernert *et al.*, 2016). The D1-M1 event was
169 followed by a greenschist facies retrograde metamorphism and D2 upright E-W folding of the
170 entire sequence (Chopin *et al.*, 2014). This late tectonic event was probably contemporaneous
171 with the intrusion of the Ras El Abiod granitoid (Baudin *et al.*, 2003). The M1 Barrovian and
172 M2 retrograde metamorphic events were dated at 310–295 Ma and 295–285 Ma, respectively
173 using $^{40}\text{Ar}/^{39}\text{Ar}$ (micas, amphiboles) and U–Pb (monazite) techniques (Chopin *et al.*, 2014;

174 Wernert *et al.*, 2016). Late to Post orogenic felsic magmatism (Piqué, 1979; Lagarde *et al.*,
175 1989) is represented by the intrusions of the Sebt Brikiyine granite (Fig. 2) dated at ca. 275 Ma
176 (e.g. Chopin *et al.*, 2014 and reference therein).

177 **Methods - zircon separation, imaging and measurements**

178 Two to four kilograms of rock per sample were processed at the laboratories of Czech
179 Geological Survey in Prague. The zircon grains were separated by sieving (0.2 and 0.1 mm),
180 heavy liquid (acetylene tetrabromide and methylene iodide) and magnetic separation. Then,
181 they were selected randomly from the zircon concentrates by hand-picking under binocular
182 microscope. The grains were mounted in epoxy discs, ground and polished.
183 Cathodoluminescence (CL) and secondary electrons imaging were performed at the SEM
184 Laboratory of the Czech Geological Survey (FEG-SEM TESCAN MIRA3 GMU working at 15
185 kV and ~22 mm working distance) in order to visualize internal zircon texture and zoning
186 patterns of individual grains. We tried to get around 150 analyzes per sample which allowed to
187 obtain representative and statistically significant age populations after discordant analyses are
188 removed (Vermeesch, 2004).

189 The U–Pb dating of zircon grains was performed at the laboratories of the Czech
190 Geological Survey. Measurements were performed on an Analyte Excite 193 nm excimer laser-
191 ablation system (LA; Photon Machines), equipped with a two-volume HeEx ablation cell, in
192 tandem with an Agilent 7900x ICPMS (Agilent Technologies Inc., Santa Clara, USA). Samples
193 were ablated in He atmosphere (0.8 l min^{-1}) at a pulse repetition rate of 10 Hz using a spot size
194 of 25 μm and laser fluence of 4.71 J cm^{-2} . Each measurement consisted of 20 seconds of blank
195 acquisition followed by ablation of the sample for a further 40 seconds of signal collection at
196 masses 202, 204, 206, 207, 208, 232 and 238 using the SEM detector, with one point per mass
197 peak and the respective dwell times of 10, 10, 15, 30, 20, 10 and 15 milliseconds per mass (total
198 sweep time of 0.134 seconds). Instrumental drift was monitored by repeated measurements of

199 the 91500 (ca. 1063 Ma, Wiedenbeck *et al.*, 1995) reference zircon. Data deconvolution using
200 Iolite software followed the method described by Paton *et al.* (2010), including an ‘on peak’
201 gas blank subtraction followed by correction for laser-induced elemental fractionation (LIEF)
202 by comparison with the behaviours of the 91500 reference zircon (Wiedenbeck *et al.*, 1995)
203 which yielded a concordia age at 1062.6 ± 1.6 Ma. No common Pb correction was applied in
204 this study. In addition, zircon reference samples GJ-1 (~609 Ma; Jackson *et al.*, 2004) and
205 Plešovice (~337 Ma; Sláma *et al.*, 2008) were analysed periodically during this study and
206 yielded concordia ages at 609.3 ± 1.5 Ma and 338.5 ± 1.0 Ma (2σ), respectively.

207 The analytical data were plotted using the IsoplotR toolbox (Vermeesch, 2018). Data
208 reduction followed the recommendation of Spencer *et al.* (2016) whereby data is treated as
209 concordant if the 2σ ellipse overlaps with the concordia, and the preferred ages are single zircon
210 concordia ages following the recommendations of Nemchin and Cawood (2005) and
211 Zimmermann *et al.* (2018). For all concordant ages younger than 1000 Ma the $^{206}\text{Pb}/^{238}\text{U}$ ages
212 were used, whereas older ages are based on the obtained $^{207}\text{Pb}/^{206}\text{Pb}$ ratios (Gehrels, 2012). We
213 kept U–Pb zircon ages with a degree of concordance situated in between 95% and 105% which
214 corresponds to the number of analyzed zircon needed to get sufficient representative data.

215 **4.Results**

216 In this study, we collected early Cambrian to Mississippian (meta)sandstone samples from eight
217 sites for U–Pb detrital zircon geochronology. From each location, we took several pieces of
218 rock from the main sedimentary strata to ensure the representativeness of the sampling. The
219 geographic, geological and stratigraphic characteristics of each sampling sites are shown in
220 figures 2 and 3, and table 1. Note that no zircon grain were found after mineral separation of
221 (meta)clastic rocks samples from the Draa El Kebir, Kef El Mouneb and Lalla Tittaf
222 Formations. Therefore, only five age spectra are presented in the following.

223 **Sample R16-1A**

224 The sample R16-1A was collected at the southern border of the Sebt Brikiyine granitic intrusion
225 (Fig. 2). It is an early Cambrian arkosic metasandstone overlying the Paleoproterozoic
226 basement (Pereira *et al.*, 2015) with an essentially preserved unconformable stratigraphic
227 contact, which was, however, possibly tectonically reactivated (Fig. 3, Fig. 4a). This deformed
228 arkosic metasandstone (Fig. 4b) is composed of equigranular fine-grained quartz grains with
229 well equilibrated straight boundaries ranging from 60 to 500 μm in size. Feldspar and muscovite
230 grains show incipient recrystallization (Fig. 5a). Polygonal zircon grains with angular shape are
231 120–200 μm grains size while sub-rounded grains of irregular shape are smaller ($<50 \mu\text{m}$).
232 Most of zircon grains show homogeneous cores surrounded by a brighter oscillatory domain
233 (CL-light) and darker rim (CL-dark; Fig. 6a). The grains are commonly fractured. One hundred
234 seventeen concordant ages from 230 analyses were obtained (Fig. 7a), showing a unimodal
235 Paleoproterozoic age spectrum (Fig. 7b) peaking at ca. 2000–2100 Ma (mean age 2048.3 ± 1.4
236 Ma).

237 **Sample SK1-Z**

238 The sample SK1-Z was collected from a quartzitic level surrounded by low grade schist of the
239 Ordovician-Devonian (?) Skhour Formation (Fig. 2, Fig. 3, Fig. 4c). This highly deformed
240 quartzite is characterized by well equilibrated quartz foam texture with subequant quartz grains
241 150–200 μm in size with straight boundaries and an excellent triple point network. (Fig. 5b).
242 The zircon population consists of elongated, sub-euhedral to euhedral grains 140–180 μm in
243 size and few more rounded smaller grains 60–100 μm in size. The analyzed zircon grains are
244 characterized by a prismatic and sector zoning with some fractures and inclusions (Fig. 6b).
245 Ninety-four concordant ages from 123 analyses were obtained (Fig. 8a). Cryogenian-Ediacaran
246 ages (540–850 Ma) constitutes 73% of all analyses with a peak at ca. 626 Ma. There are very

247 subordinate clusters at 1700–2200 Ma (18%) and another one at ca. 1 Ga (1%). A small peak
248 at ca. 580 Ma is also present (Fig. 8a).

249 **Sample R257-OH**

250 R257-OH was collected in quartzite lenses of the eastern extremity of the OH-OZ Formation
251 (near the Souk el Had; Fig. 2, Fig. 3). The formation can be either Lower or Middle to Upper
252 Devonian (El Houicha *et al.*, 2019) depending on the interpretation of the stratigraphic polarity
253 (e.g. Hoepffner, 1974; Cornée, 1982; Razin *et al.*, 2003). These weakly metamorphosed and
254 deformed impure quartzite (Fig. 4d) is composed of recrystallized, elongate grains of quartz
255 with lobate boundaries and irregular undulatory extinction and minor recrystallized muscovite
256 (Fig. 5c). Large detrital zircon grains (100–150 μm) have a long prismatic shape whereas
257 smaller zircon population (50–75 μm in size) are sub-rounded. Most of the large zircons show
258 a sector zoning but some are characterized by prismatic zonation patterns (Fig. 6c). Several
259 rounded grains are homogeneous and weakly luminescent. A set of 138 concordant ages has
260 been obtained from 161 analyses (Fig. 8a). They show a main Cryogenian-Ediacaran population
261 (540–850 Ma; 79%) with a peak at ca. 632 Ma and a smaller Paleoproterozoic cluster (1700–
262 2200 Ma; 17%) with two peaks at ca. 1764 and 2071 Ma. Distributed Mesoproterozoic and
263 Archean ages are also present (Fig. 8b).

264 **Sample R255-OZ**

265 The sample R255-OZ was collected next to the fossiliferous Eifelian-Frasnian limestones
266 (El Houicha *et al.*, 2019) of the OH-OZ Formation along the Ouled-Zednes Fault zone (Fig. 2,
267 Fig. 3). The site shows a narrow belt of steeply SE-dipping quartzite, shale and limestone of the
268 OH-OZ Formation surrounded by Skhour Formation rocks in the northwest and Koudiat El
269 Adam rocks in the SE (Fig. 4g,e). The sampled rock is a light-grey low-grade quartzite (Fig.
270 4f) showing incipient bulging type recrystallization at margins of detrital quartz grains (100 to
271 200 μm in size) and presence of small sericite grains (Fig. 5d). The age of this rock is probably

272 Upper Devonian (post-Frasnian) to Dinantian in stratigraphic continuity with the Middle
273 Devonian Ouled Zednes Formation of the lower metamorphic unit (Jenny, 1974; Razin, 2003;
274 Baudin et al., 2003). However, Baudin *et al.* (2003) did not exclude that it might represent a
275 tectonic slice from the upper metamorphic unit, either from the western Cambro-Ordovician or
276 Upper Devonian Skhour Formation, or from the eastern Ordovician Jbel Kharrou-Koudiat El
277 Adam nappe (Fig. 2). The zircon grains reveal a complex texture in their CL images with
278 variable luminescence and patterns. Most of the extracted detrital zircon from this sample is
279 about 60–100 μm in size, showing oscillatory or sector zoned with irregular or straight grain
280 boundaries. Less frequently, low- to high luminescent homogenous elongated grains 120–140
281 μm in size are present (Fig. 6d). One hundred twenty-two concordant ages from 178 analyses
282 have been obtained from this sample (Fig. 8c). They show multimodal age spectra ranging
283 between 310–540 Ma (13%), 540–850 Ma (52%), 850–1200 Ma (15%) and 1500–2200 Ma
284 (15%). A younger population shows subordinate peaks at 477 and 559 Ma. Nevertheless, the
285 youngest detrital zircon ages are close to 350 Ma (Fig. 6d, Fig. 8c).

286 **Sample R256-DT**

287 The sample R256-DT was collected from the Dalaat unit (member 2 in the Dalaat Formation
288 s.s.; Razin *et al.*, 2003; Fig. 2; Fig. 3). This unit corresponds to middle (?)–late Visean basal
289 fine to medium grained arkosic sandstones alternating with limestone (Fig. 4h,i). The sandstone
290 is composed of quartz and feldspar grains, 150–400 μm in size, some detrital muscovite,
291 chloritized biotite and interstitial calcite (Fig. 5e). The zircon grains show either subhedral
292 shapes and oscillatory and sector zoning or sub-rounded shapes and homogeneous weakly or
293 highly luminescent patterns (Fig. 6e). The studied zircon grain size falls primarily into the 120–
294 170 μm range and less frequently into the 60–100 μm range. A total of 182 analyses were
295 carried out, of which 136 displayed concordant ages (Fig. 8d). The sample R256-DT is
296 dominated by a Cryogenian-Ediacaran population (68%) ranging between 540 and 850 Ma with

297 a peak at 633.9 ± 0.5 Ma and three subordinate populations at 850–1200 Ma (12%), 1500–2200
298 Ma (13%) and 2200–2500 Ma (13%) suggesting potential peaks around 991 Ma, 1943 Ma and
299 2446 Ma, respectively (Fig. 8b).

300 Most of the analyses from all the samples are characterized by Th/U ratios > 0.1 (ranging
301 between 0.1 and 1.7) suggesting a primary magmatic origin (Rubatto, 2002). However, some
302 zircon rims show Th/U ratios lower than 0.1, in particular those in the 600–850 Ma range, which
303 is compatible with a metamorphic remobilization.

304 **5. Discussion**

305 **Evolution of detrital zircon sources in time**

306 South of the Sebt Brikiyine granite, Pereira *et al.* (2015) described an Eburnean basement dated
307 at 2050.6 ± 3.0 Ma (SHRIMP U–Th–Pb, rhyolitic porphyry, sample SBR-21 in Fig. 2 and Fig.
308 3). The basement is unconformably overlain by clastic (pelites, arkoses) and carbonate
309 (limestones and calcschists) strata similar to the early Cambrian succession outcropping in the
310 northern Lalla Mouchaa Formation and in the Sidi Ali dome in the lower metamorphic unit of
311 the Central Rehamna (Corsini *et al.*, 1988). The sample R16-1A (Fig. 2), an arkosic sandstone
312 directly overlying the Paleoproterozoic basement, only show zircon grains with
313 Paleoproterozoic ages (mean age 2048.3 ± 1.4 Ma). This cluster is similar to the one obtained
314 from early Cambrian microbreccia from the Lalla Mouchaa Formation (Sample NB1; Fig. 2,
315 Fig. 3) with detrital zircons at ca. 2047 ± 12 Ma (El Houicha *et al.*, 2018). Both samples (R16-
316 1A, this study, and NB1, El Houicha *et al.*, 2018) are characterized by angular feldspar and
317 euhedral zircons, the latter with concentric zoning suggesting a magmatic origin and a low
318 roundness indicative for a very short transport distance and thus, low-order recycling of
319 sediments. Correlation with published ages shows that the detrital zircon likely derived from
320 first-cycle erosion of the local Eburnean basement (Pereira *et al.*, 2015) indicating proximal

321 watersheds collecting the signal from the nearby rocks (Fig. 9a). At regional scale, the detrital
322 zircons from the basal early Cambrian sediments overlying the Meseta basement reflect
323 exclusive, local recycling of the heterogeneous Precambrian basement. Indeed, detrital zircons
324 ages from the early Cambrian microbreccia at Lalla Mouchaa and (meta)arkose from south of
325 Sebt Brikiyine granite are perfectly similar to the age of the underlying rhyolitic basement
326 (2050.6 ± 3.0 Ma, sample SBR-21 in Pereira *et al.*, 2015). Similarly, a single Cadomian/Pan-
327 African cluster is found in detrital zircon from the early Cambrian microbreccia (ca. 583,
328 sample JD2) covering the El Jadida rhyolitic basement dated at 584.2 ± 4.8 Ma, sample JD-1
329 in El Houicha *et al.*, 2018). Finally, the Neoproterozoic metavolcanic rocks from the Sidi Ali
330 Dome (593 ± 8 Ma, Baudin *et al.*, 2003) is covered by early Cambrian metaconglomerates
331 containing granitic pebbles showing zircon ages in the range 600–640 Ma (Pereira *et al.* (2014),
332 whereas detrital zircons ages from the matrix are in the range 548–624 Ma (Sample 15DL11 in
333 Letsch *et al.*, 2018). This discrimination between Eburnean and Cadomian/Pan-African
334 basements and sources in the Western Meseta, might reflect an inherited suture zone originating
335 the WMSZ since the early Paleozoic (e.g. Piqué *et al.*, 1980, Corsini, 1991).

336 Samples SK1-Z (upper metamorphic unit) and R257-OH (lower metamorphic unit) show
337 very similar density probability curves, largely dominated by a Cryogenian-Ediacaran
338 population, including a late Ediacaran subpopulation. Additionally, there is a Paleoproterozoic
339 population ranging between 1700–2200 Ma. The main Pan-African peak with moderate
340 Paleoproterozoic ages is typical of West African Cambrian to Devonian age spectra (Gärtner *et*
341 *al.*, 2017; Letsch *et al.*, 2018; Ghienne *et al.*, 2018; Accotto *et al.*, 2021b). Similar age
342 populations might indicate that those two samples originally belong to the same stratigraphic
343 unit: the Devonian stratigraphic age of the R257-OH sample (Fig. 2, Fig. 3) might therefore
344 suggest that the SK1-Z sample is also from a Devonian unit, as proposed by Baudin *et al.* (2003)
345 and Michard *et al.* (2010). However, detrital zircon data from the Central massif (Accotto *et*

346 *al.*, 2021b) show that such an age spectrum does not allow differentiating Ordovician from
347 Devonian strata and that similar zircon populations are identified in both the Ordovician of
348 some of the autochthonous strata (Ezzhelligha area, EZ on the Fig. 1) and allochthonous strata
349 (Azrou area, AZR on the Fig. 1). Nevertheless, because sample SK1-Z has affinities with both
350 Ordovician samples from the Ezzhelligha area (Accotto *et al.*, 2021b) and the late Cambrian
351 (El Hank) from the nearby Coastal Block (sample 15DL12, IMF on the Fig. 1) (Letsch *et al.*,
352 2018), we favor an Ordovician age for the SK1-Z rock unit, and not favor an Upper Devonian
353 age as suggested by Baudin *et al.* (2003) and Michard *et al.* (2010). Whatever the stratigraphic
354 attribution of the samples might be, SK1-Z and R257-OH and similar ones from the Meseta
355 show that the southern-derived West Gondwana source (i.e. dominant Cadomian/Pan-African
356 and Eburnean source) essentially pertained from the Cambrian-Ordovician up to the Devonian
357 (Fig. 9b; Gärtner *et al.*, 2017; Accotto *et al.*, 2021b). The minor presence of Meseoproterozoic
358 zircons, also described elsewhere in the Meseta might reflect a minor lateral source from the
359 Sahara Metacraton (see however discussion in Accotto *et al.*, 2021b).

360 The sample R255-OZ collected in the OH-OZ Formation shows a major change with two
361 grains indicating a maximum depositional age as young as early Carboniferous (350.6 ± 10 Ma
362 and 352.5 ± 7 Ma, i.e. Tournaisian), i.e. significantly younger than the Devonian strata hosting
363 the sample R257-OH. This is in full agreement with a distinctive age spectrum, showing
364 Ordovician to Lower Devonian subordinate peaks and a less prominent Pan-African population.
365 As in R256-DT (see next paragraph), Mesoproterozoic zircon grains are present but more
366 distributed within the Mesoproterozoic instead of a peak at ~ 1 Ga. It suggests a different
367 sourcing, confirmed by the morphology of zircons which are mostly euhedral and poorly
368 rounded—in contrast to detrital zircons from the underlying Cambrian to Devonian strata—,
369 indicating a relatively short transportation path. If the Cambrian to Lower Ordovician zircon
370 grains can be derived from nearby sedimentary sources (Letsch *et al.*, 2018; Accotto *et al.*,

371 2021b), again indicating the recycling of the Meseta early Paleozoic sedimentary cover,
372 occurrences of late Paleozoic and Mesoproterozoic zircon grains suggests in addition great
373 changes in the distribution of the watersheds. In particular, the latter are well known to include
374 renewed volcanic activity at the regional scale (Kharbouch, 1994; Moreno *et al.*, 2008; Aït
375 Lahna *et al.*, 2018). The source of Mesoproterozoic zircons might reflect the presence of an
376 allochthonous unit positioned to the north and docked in the course of the Variscan collision as
377 suggested from studies in the Eastern Meseta (e.g. Accotto *et al.*, 2020b). However, the limited
378 number of “Variscan” late Paleozoic zircons grains in the Rehamna massif, which are largely
379 more represented in the Eastern Meseta, makes this sourcing from the northern watersheds
380 unlikely. On the other hand, the sediment transport scenario from the WAC cannot be excluded.
381 The samples R255-OZ and R256-DT show some increased Mesoproterozoic component which
382 is well known from the sedimentary cover of the western edge of the WAC (Taoudeni basin;
383 Bradley *et al.*, 2015; Gärtner *et al.*, 2017). Moreover, detrital zircon data indicates a dispersal
384 of Mesoproterozoic detritus since Cambrian times (e.g. Gärtner *et al.*, 2017; Fig 10b).
385 Derivations from either the southwest, running parallel to the continental margin and the
386 coevally forming orogen, or from the northwest (Avalonia or European Variscan Orogen; i.e.,
387 orthogonal to the Variscan collision) might be postulated.

388 The middle (?)–late Visean sample R256-DT collected from the basal siliciclastic Dalaat
389 Formation is also dominated by Ediacaran to Cryogenian ages but with other subordinate, yet
390 significant signals: distributed Mesoproterozoic zircon grains, a small but definite Stenian-
391 Tonian peak, and a early Cryogenian subpopulation. It may be interpreted as a continuum of
392 the Cambrian-Ordovician source, with addition of subordinate new sources, or, alternatively,
393 as the recycling of Meseta-derived Cambrian-Devonian strata (Fig. 9d) because all of the
394 additional signals are also present, admittedly in various proportion, in Lower Paleozoic strata
395 outcropping in the Meseta, and more specifically in northern and north-eastern Meseta

396 (Ghienne *et al.*, 2018; Accotto *et al.*, 2020a; 2021). A combination of the two schemes, a
397 western Gondwana source combined with the recycling of older strata, is in fact likely.

398 **Geodynamic implications**

399 This study indicates a modification through time of detrital sources feeding the
400 continental shelf and the sedimentary basins in the current Rehamna area, which is compatible
401 with the geodynamic model recently proposed for the Variscan belt (Martínez Catalán *et al.*,
402 2021). The reconstructions based on existing paleomagnetic and geological data and models of
403 Domeier and Torsvik (2014) and Matthews *et al.* (2016) allow to visualize evolution of zircon
404 sources as suggested in this work, in complementing and agreeing with the study of Accotto *et*
405 *al.* (2021a). Since the Ordovician, the northern Gondwana has evolved in a passive margin
406 setting, suggesting that the detrital zircon populations deposited in Ordovician to Lower
407 Devonian basins were entirely governed by recycling Gondwanan sources from the south and
408 SE, represented either by remote exposed basements, and/or their sedimentary covers (Fig.
409 10a). However, the situation radically changed owing to two separate late Devonian to early
410 Carboniferous events. The first one is related to the propagation of the Paleotethys ocean
411 (Stampfli *et al.*, 2003; Stampfli *et al.*, 2013) into the interior of Gondwana thereby forming the
412 network of basins typical for Eastern and Western Meseta (Cózar *et al.*, 2020) and oceanic
413 realm further east (Edel *et al.*, 2018; Fig. 10b), which is typified in the Rehamna massif by the
414 formation of the Devonian to early Carboniferous basins and associated magmatism
415 (Hoepffner, 1974; 1982; Aït Lahna *et al.*, 2018). At the same time, a ribbon fragment of
416 Gondwana called the Mid-Variscan Autochthon was obducted by giant allochthonous nappe
417 complexes (Martínez Catalán *et al.*, 2021) involving both oceanic and continental rocks (Fig.
418 10b). This event occurred simultaneously with possible westward indentation of Avalonian
419 promontory with the Variscan autochthon as discussed by Accotto *et al.* (2021a). It was recently
420 shown that the Mid-Variscan allochthon also contains sedimentary sequences with abundant

421 Mesoproterozoic zircon signature (Lindner *et al.*, 2021) previously considered as typical for
422 Avalonia (Mazur *et al.*, 2010).

423 Therefore, the opening of Lower Devonian to Carboniferous sedimentary basins within
424 the Moroccan Meseta was coeval with a major convergent event in the north. In this context,
425 Mesoproterozoic zircons grains of the late Paleozoic Rehamna record are thought to have
426 principally originated from the convergent deformation zone, derived from either an Avalonian
427 (e.g. Gärtner *et al.*, 2018) or mid-Allochthonous (e.g. Lindner *et al.*, 2021) source, even though
428 the massive peak at 1.3 Ga from the latter could be “diluted” in our samples. Indeed, a
429 contribution through recycling of the sedimentary cover of the WAC cannot be totally excluded.
430 Anyway, the source of Mesoproterozoic zircons from the Variscan core and/or Avalonian
431 indenter (Accotto *et al.*, 2021a) remain questionable as the early Carboniferous paleo-
432 geographic position of both possible source areas remains poorly constrained. To the contrary,
433 early Carboniferous zircon grains (sample R255-OZ) are argued to principally derived from
434 early Carboniferous magmatism reported in the Moroccan Meseta (Kharbouch, 1994), although
435 we note that the Mid-Variscan Allochthon was intruded by series of magmatic arcs from 380
436 to 350 Ma (e.g. Lardeaux *et al.*, 2014; Deiller *et al.*, 2021) which could have also contributed
437 to the detrital zircon record in the Rehamna basin.

438 **Acknowledgments**

439 The authors want to gratefully acknowledge Nikol Novotná (SEM laboratory) and the
440 technician from the Czech Geological Survey involved in the preparation of the samples. This
441 work was supported by the TelluS Program of CNRS/INSU and institutional grants from the
442 Czech Geological Survey (grant number 310270 and DKRVO) and from the CNRS IPGS
443 UMR7516 (now ITES UMR 7063). The University Chouaïb Doukkali and Martin Simon are
444 thanked for their support during the field work. Fabien Humbert (Southern University of
445 Science and Technology, Shenzhen) is thanked for the processing of photographs.

447 **References**

- 448 Accotto, C., Martínez Poyatos, D.J., Azor, A., Talavera, C., Evans, N.J., Jabaloy-Sánchez, A.,
 449 Azdimousa, A., Tahiri, A., El Hadi, H., 2019. Mixed and recycled detrital zircons in the
 450 Paleozoic rocks of the Eastern Moroccan Meseta: Paleogeographic inferences. *Lithos*,
 451 338–339, 73–86. <https://doi.org/10.1016/j.lithos.2019.04.011>
- 452 Accotto, C., Martínez Poyatos, D., Azor, A., Jabaloy-Sánchez, A., Talavera, C., Evans, N.J.,
 453 Azdimousa, A., 2020. Tectonic Evolution of the Eastern Moroccan Meseta: From Late
 454 Devonian Forearc Sedimentation to Early Carboniferous Collision of an Avalonian
 455 Promontory. *Tectonics*, 39, 1–29. <https://doi.org/10.1029/2019TC005976>
- 456 Accotto, C., Martínez Poyatos, D., Azor, A., Talavera, C., Evans, N.J., Jabaloy-Sánchez, A.,
 457 Azdimousa, A., Tahiri, A., El Hadi, H., 2021a. Syn-collisional detrital zircon source
 458 evolution in the northern Moroccan Variscides. *Gondwana Research*, 93, 73–88.
 459 <https://doi.org/10.1016/j.gr.2021.02.001>
- 460 Accotto, C., Martínez Poyatos, D., Azor, A., Talavera, C., Evans, N.J., Jabaloy-Sánchez, A.,
 461 Tahiri, A., El Hadi, H., Azdimousa, A., 2021b. Systematics of detrital zircon U–Pb ages
 462 from Cambrian–Lower Devonian rocks of northern Morocco with implications for the
 463 northern Gondwanan passive margin. *Precambrian Research*, 365.
 464 <https://doi.org/10.1016/j.precamres.2021.106366>
- 465 Accotto, C., Martínez Poyatos, D., Azor, A., Talavera, C., Evans, N.J., Jabaloy-Sánchez, A., El
 466 Hadi, H., Tahiri, A., 2022. Detrital zircon sources in the Ordovician metasedimentary
 467 rocks of the Moroccan Meseta: Inferences for northern Gondwanan passive-margin
 468 paleogeography, in: *New Developments in the Appalachian-Caledonian-Variscan*
 469 *Orogen*. Geological Society of America. [https://doi.org/10.1130/2021.2554\(17\)](https://doi.org/10.1130/2021.2554(17))
- 470 Aghzher, A.M., Arenas, R., 1995. Détachements et tectonique extensive dans le massif hercynien
 471 des Rehamna (Maroc). *Journal of African Earth Sciences*, 21, 383–393.
 472 [https://doi.org/10.1016/0899-5362\(95\)00096-C](https://doi.org/10.1016/0899-5362(95)00096-C)
- 473 Aït Lahna, A., Aarab, E.M., Nasrddine, Y., Colombo Celso Gaeata, T., Bensalah, M.,
 474 Boumehdi, M.A., Kei, S., Basei, M.A.S., 2018. The Lalla Tittaf Formation (Rehamna,
 475 Morocco): Paleoproterozoic or Paleozoic age?, in: *ICG2018-Joint Congress-CAAWG9-*
 476 *CAAWG9-ArabGU2-ICGAME3*, Abstract Book. El Jadida, pp. 13–16.
- 477 Avigad, D., Gerdes, A., Morag, N., Bechstädt, T., 2012. Coupled U–Pb–Hf of detrital zircons
 478 of Cambrian sandstones from Morocco and Sardinia: Implications for provenance and
 479 Precambrian crustal evolution of North Africa. *Gondwana Research*, 21, 690–703.
 480 <https://doi.org/10.1016/j.gr.2011.06.005>
- 481 Baudin, T., Chévremont, P., Razin, P., Youbi, N., Andries, D., Hoepffner, C., Thiéblemont, D.,
 482 Chihani, E., Tegye, M., 2003. Carte géologique du Maroc au 1/50 000, feuille de Skhour
 483 des Rehamna, Mémoire explicatif. Notes et Mémoires du Service Géologique du Maroc,
 484 Rabat, 435 bis, 1–114.
- 485 Bradley D.C., O’Sullivan P., Cosca M.A., Motts H.A., Horton J.D., Taylor C.D., Beaudoin G.,
 486 Lee G.K., Ramezani J., Bradley D.B., Jones J.V., Bowring S., 2015. Synthesis of
 487 geological, structural, and geochronologic data (Phase V, Deliverable 53). Chapter A of
 488 Taylor CD (ed.), *Second Projet de Renforcement Institutionnel du Secteur Minier de la*
 489 *République Islamique de Mauritanie (PRISM-II)*. U.S. Geological Survey Open-File
 490 Report 2013 12080-A, 328p. doi:10.3133/ofr20131280
- 491 Chopin, F., Corsini, M., Schulmann, K., El Houicha, M., Ghienne, J.-F., Edel, J.-B., 2014.
 492 Tectonic evolution of the Rehamna metamorphic dome (Morocco) in the context of the

- 493 Alleghanian-Variscan orogeny. *Tectonics*, 33, 1154–1177.
 494 <https://doi.org/10.1002/2014TC003539>
- 495 Cornée, J.-J., 1982. Étude lithostratigraphique et tectonométamorphique des Rehamna sud-
 496 orientales. Plissements et nappes. Contribution à la connaissance de la chaîne hercynienne
 497 en Meseta marocaine. *Trav. Lab. Sci. Terre, Saint Jérôme, Université Aix–Marseille III*,
 498 Aix-Marseille.
- 499 Corsini M., 1991. Influence de la paléogéographie du Paléozoïque sur les déformations
 500 hercyniennes de la Meseta nord-occidentale du Maroc. *Géologie Méditerranéenne*, 18,
 501 (1-2), 73–80. <https://doi.org/10.3406/geolm.1991.1453>
- 502 Corsini, M., Muller, J., Cornée, J.-J., Diot, H., 1988. Découverte de la série basale du Cambrien
 503 et de son substratum dans les Rehamna centraux, haut-fond au Cambrien (Meseta
 504 marocaine). *Prémices de l'orogénèse hercynienne. Comptes Rendus de l'Académie des*
 505 *sciences, Série II*, 306, 63–68.
- 506 Cózar, P., Vachard, D., Izart, A., Said, I., Somerville, I., Rodríguez, S., Coronado, I., El
 507 Houicha, M., Ouarhache, D., 2020. Lower-middle Viséan transgressive carbonates in
 508 Morocco: Palaeobiogeographic insights. *Journal of African Earth Sciences*, 168.
 509 <https://doi.org/10.1016/j.jafrearsci.2020.103850>
- 510 Deiller, P., Štípská, P., Ulrich, M., Schulmann, K., Collett, S., Peřestý, V., Hacker, B.,
 511 Kylander-Clark, A., Whitechurch, H., Lexa, O., Pelt, E., Míková, J., 2021. Eclogite
 512 subduction wedge intruded by arc-type magma: The earliest record of Variscan arc in the
 513 Bohemian Massif. *Gondwana Research*, 99, 220–246.
 514 <https://doi.org/10.1016/J.GR.2021.07.005>
- 515 Delchini, S., Lahfid, A., Lacroix, B., Baudin, T., Hoepffner, C., Guerrot, C., Lach, P., Saddiqi,
 516 O., Ramboz, C., 2018. The Geological Evolution of the Variscan Jebilet Massif, Morocco,
 517 Inferred From New Structural and Geochronological Analyses. *Tectonics*, 37, 4470–
 518 4493. <https://doi.org/10.1029/2018TC005002>
- 519 Destombes, J., Guézou, J.-C., Hoepffner, C., Jenny, P., Piqué, A., Michard, A., 1982. Le
 520 Primaire du massif des Rehamna s.s., problèmes de stratigraphie des séries
 521 métamorphiques, in: Michard, A. (Ed.), *Le massif Paléozoïque des Rehamna (Maroc):*
 522 *Stratigraphie, Tectonique et Petrogenese d'un segment de la Chaîne Varisque. Notes et*
 523 *Mémoires du Service Géologique, Rabat 303*, pp. 35–70.
- 524 Domeier, M., Torsvik, T.H., 2014. Plate tectonics in the late Paleozoic. *Geoscience Frontiers*,
 525 5, 303–350. <https://doi.org/10.1016/j.gsf.2014.01.002>
- 526 Edel, J.-B., Schulmann, K., Lexa, O., Lardeaux, J.M., 2018. Late Palaeozoic palaeomagnetic
 527 and tectonic constraints for amalgamation of Pangea supercontinent in the European
 528 Variscan belt. *Earth-Science Reviews*, 177, 589–612.
 529 <https://doi.org/10.1016/j.earscirev.2017.12.007>
- 530 El Hassani, A., 1991. La Zone de Rabat-Tiflet: bordure nord de la Chaîne Calédono-
 531 Hercynienne du Maroc. *Bulletin de l'Institut Scientifique, Rabat*, 15, 1–34.
- 532 El Houicha, M., Aboussalam, Z.S., Rodriguez, S., Chopin, F., Jouhari, A., Schulmann, K.,
 533 Ghienne, J-F., Becker, R.T., 2019. Discovery of Eifelian-Frasnian corals in metamorphic
 534 rocks from the Rehamna massif (Moroccan Meseta): biostratigraphic and
 535 paleogeographic implications. 11th Colloquium 3MA « Magmatism, Metamorphism and
 536 associated Mineralization », 38–40.
- 537 El Houicha, M., Pereira, M.F., Jouhari, A., Gama, C., Ennih, N., Fekkak, A., Ezzouhairi, H., El
 538 Attari, A., Silva, J.B., 2018. Recycling of the Proterozoic crystalline basement in the
 539 Coastal Block (Moroccan Meseta): New insights for understanding the geodynamic
 540 evolution of the northern peri-Gondwanan realm. *Precambrian Research*, 306, 129–154.
 541 <https://doi.org/10.1016/j.precamres.2017.12.039>

- 542 El Kamel, F., 2002. Sédimentologie, magmatisme pré-orogénique et structuration du
543 Paléozoïque des Rehamna et d'Ouled Abbou (Meseta occidentale, Maroc). Thèse,
544 Doctorat ès-Sciences, Université Hassan II, Casablanca, Maroc, 208 p.
- 545 El Mahi, B., Hoepffner, C., Zahraoui, M., Boushaba, A., 1999. L'évolution structurale et
546 métamorphique de la zone hercynienne des Rehamna centraux (Maroc). GAW 4,
547 International Conference on Geology of the Arab World, Cairo University, Egypt, pp.
548 26–45.
- 549 Frizon de Lamotte, D., Tavakoli-Shirazi, S., Leturmy, P., Averbuch, O., Mouchot, N., Raulin,
550 C., Leparmentier, F., Blanpied, C., Ringenbach, J.-C., 2013. Evidence for Late Devonian
551 vertical movements and extensional deformation in northern Africa and Arabia:
552 Integration in the geodynamics of the Devonian world. *Tectonics*, 32, 107–122.
553 <https://doi.org/10.1002/tect.20007>
- 554 Gärtner, A., Villeneuve, M., Linnemann, U., El Archi, A., Bellon, H., 2013. An exotic terrane
555 of Laurussian affinity in the Mauritanides and Souttoufides (Moroccan Sahara).
556 *Gondwana Research*, 24, 687–699. <https://doi.org/10.1016/j.gr.2012.12.019>
- 557 Gärtner, A., Youbi, N., Villeneuve, M., Sagawe, A., Hofmann, M., Mahmoudi, A., Boumehdi,
558 M.A., Linnemann, U., 2017. The zircon evidence of temporally changing sediment
559 transport—the NW Gondwana margin during Cambrian to Devonian time (Aoucert and
560 Smara areas, Moroccan Sahara). *International Journal of Earth Sciences*, 106, 2747–2769.
561 <https://doi.org/10.1007/s00531-017-1457-x>
- 562 Gärtner, A., Youbi, N., Villeneuve, M., Linnemann, U., Sagawe, A., Hofmann, M., Zieger, J.,
563 Mahmoudi, A., Boumehdi, M.A., 2018. Provenance of detrital zircon from siliciclastic
564 rocks of the Sebkhha Gezmayet unit of the Adrar Souttoug Massif (Moroccan Sahara) –
565 Palaeogeographic implications. *Comptes Rendus Geoscience*, 350, 255–266.
566 <https://doi.org/10.1016/j.crte.2018.06.004>
- 567 Gehrels, G., 2012. Detrital Zircon U-Pb Geochronology: Current Methods and New
568 Opportunities, in: *Tectonics of Sedimentary Basins*. John Wiley & Sons, Ltd, Chichester,
569 UK, pp. 45–62. <https://doi.org/10.1002/9781444347166.ch2>
- 570 Ghienne, J.F., Benvenuti, A., El Houicha, M., Girard, F., Kali, E., Khoukhi, Y., Langbour, C.,
571 Magna, T., Míková, J., Moscariello, A., Schulmann, K., 2018. The impact of the end-
572 Ordovician glaciation on sediment routing systems: A case study from the Meseta
573 (northern Morocco). *Gondwana Research*, 63, 169–178.
574 <https://doi.org/10.1016/j.gr.2018.07.001>
- 575 Guézou, J.-C., Michard, A., 1976. Note sur la structure du môle côtier mésétien dans l'ouest
576 des Rehamna (Maroc hercynien). *Sciences Géologiques, Bulletin, Strasbourg*, 29,
577 171–182.
- 578 Hanchar, J.M., Miller, C.F., 1993. Zircon zonation patterns as revealed by
579 cathodoluminescence and backscattered electron images: Implications for interpretation
580 of complex crustal histories. *Chemical Geology*, 110, 1–13. [https://doi.org/10.1016/0009-2541\(93\)90244-D](https://doi.org/10.1016/0009-2541(93)90244-D)
- 582 Hoepffner, C., 1974. Contribution à la géologie structurale des Rehamna (Meseta marocaine
583 méridionale), le matériel paléozoïque et son évolution hercynienne dans l'est du massif.
584 Thèse 3ème cycle, Université Louis Pasteur, Strasbourg, France.
- 585 Hoepffner, C., 1987. La tectonique hercynienne dans l'Est du Maroc. Thèse ès sciences,
586 Université Louis Pasteur, Strasbourg, France.
- 587 Hoepffner, C., Jenny, P., Piqué, A., Michard, A., 1982. Le métamorphisme hercynien dans le
588 massif des Rehamna, in: Michard, A. (Ed.), *Le massif Paléozoïque des Rehamna (Maroc):*
589 *Stratigraphie, Tectonique et Petrogenese d'un segment de la Chaîne Varisque. Notes et*
590 *Mémoires du Service Géologique, Rabat*, 303, pp. 130–149.

- 591 Hoepffner, C., 1982. Le magmatisme pré- et post-orogénique hercynien dans le massif des
592 Rehamna, in: Michard, A. (Ed.), Le massif Paléozoïque des Rehamna (Maroc):
593 Stratigraphie, Tectonique et Petrogenese d'un segment de la Chaîne Varisque. Notes et
594 Mémoires du Service Géologique, Rabat, 303, pp. 150–163.
- 595 Hoepffner, C., Soulaïmani, A., Piqué, A., 2005. The Moroccan Hercynides. *Journal of African*
596 *Earth Sciences*, 43, 144–165. <https://doi.org/10.1016/j.jafrearsci.2005.09.002>
- 597 Hollard, H., Michard, A., Jenny, P., Hoepffner, C., Willefert, S., 1982. Stratigraphie du Primaire
598 de Mechra-Ben-Abbou, Rehamna, in: Michard, A. (Ed.), Le massif Paléozoïque des
599 Rehamna (Maroc): Stratigraphie, Tectonique et Petrogenese d'un segment de la Chaîne
600 Varisque. Notes et Mémoires du Service Géologique, Rabat, 303, pp. 12–34.
- 601 Jackson, S.E., Pearson, N.J., Griffin, W.L., Belousova, E.A., 2004. The application of laser
602 ablation-inductively coupled plasma-mass spectrometry to in situ U-Pb zircon
603 geochronology. *Chemical Geology*, 211, 47–69.
604 <https://doi.org/10.1016/j.chemgeo.2004.06.017>
- 605 Jenny, P., 1974. Contribution à la géologie structurale des Rehamna (Meseta marocaine
606 méridionale). Le matériel paléozoïque et son évolution hercynienne dans le centre du
607 massif. Thèse 3ème cycle, Université Louis Pasteur, Strasbourg, France.
- 608 Kharbouch, F., 1994. Le volcanisme dévono-dinantien du Massif central et de la Meseta
609 orientale. *Bulletin de l'Institut Scientifique, Rabat*, 18, 192–200.
- 610 Lagarde, J.-L., Ait Ayad, N., Ait Omar, S., Chemsseddoha, A., Saquaque, A., 1989. Les plutons
611 granitiques tardi carbonifères marqueurs de la déformation crustale. L'exemple des
612 granitoïdes de la méseta marocaine. *Comptes Rendus de l'Académie des sciences, Série*
613 *II*, 309, 291–296.
- 614 Lardeaux, J.-M., Schulmann, K., Faure, M., Janoušek, V., Lexa, O., Skrzypek, E., Edel, J.-B.
615 and Štípská, P., 2014. The moldanubian zone in the French Massif Central,
616 Vosges/Schwarzwald and Bohemian Massif revisited: differences and similarities.
617 *Geological Society, London, Special Publications*, 405(1), 7–44.
618 <http://dx.doi.org/10.1144/SP405.14>,
- 619 Letsch, D., El Houicha, M., von Quadt, A., Winkler, W., 2018. A missing link in the peri-
620 Gondwanan terrane collage: The Precambrian basement of the Moroccan Meseta and its
621 lower Paleozoic cover. *Canadian Journal of Earth Sciences*, 55, 33–51.
622 <https://doi.org/10.1139/cjes-2017-0086>
- 623 Lindner, M., Dörr, W., Reither, D., Finger, F., 2021. The Dobra Gneiss and the Drosendorf Unit
624 in the southeastern Bohemian Massif, Austria: West Amazonian crust in the heart of
625 Europe. *Geological Society, London, Special Publications*, 503, 185–207.
626 <https://doi.org/10.1144/SP503-2019-232>
- 627 Martínez Catalán, J.R., Schulmann, K., Ghienne, J.F., 2021. The Mid-Variscan Allochthon:
628 Keys from correlation, partial retro deformation and plate-tectonic reconstruction to
629 unlock the geometry of a non-cylindrical belt. *Earth-Science Reviews*, 220.
630 <https://doi.org/10.1016/j.earscirev.2021.103700>
- 631 Matthews, K.J., Maloney, K.T., Zahirovic, S., Williams, S.E., Seton, M., Müller, R.D., 2016.
632 Global plate boundary evolution and kinematics since the late Paleozoic. *Global and*
633 *Planetary Change*, 146, 226–250. <https://doi.org/10.1016/j.gloplacha.2016.10.002>
- 634 Mazur, S., Kröner, A., Szczepański, J., Turniak, K., Hanžl, P., Melichar, R., Rodionov, N. V.,
635 Paderin, I., Sergeev, S.A., 2010. Single zircon U-Pb ages and geochemistry of granitoid
636 gneisses from SW Poland: Evidence for an Avalonian affinity of the Brunian
637 microcontinent. *Geological Magazine*, 147, 508–526.
638 <https://doi.org/10.1017/S001675680999080X>

- 639 Michard, A., 1982. Le massif Paléozoïque des Rehamna (Maroc) : Stratigraphie, Tectonique et
640 Petrogenese d'un segment de la Chaîne Varisque. Notes et Mémoires du Service
641 Géologique du Maroc, Rabat, 303, 1–180.
- 642 Michard, A., Soulaïmani, A., Hoepffner, C., Ouanaïmi, H., Baïdier, L., Rjimati, E.C., Saddiqi,
643 O., 2010. The South-Western Branch of the Variscan Belt: Evidence from Morocco.
644 Tectonophysics, 492 (1–4), 1–24. <https://doi.org/10.1016/j.tecto.2010.05.021>
- 645 Moreno, C., Sáez, R., González, F., Almodóvar, G., Toscano, M., Playford, G., Alansari, A.,
646 Rziki, S., Bajddi, A., 2008. Age and depositional environment of the Draa Sfar massive
647 sulfide deposit, Morocco. Mineralium Deposita, 43, 891–911.
648 <https://doi.org/10.1007/s00126-008-0199-x>
- 649 Nemchin, A.A., Cawood, P.A., 2005. Discordance of the U–Pb system in detrital zircons:
650 Implication for provenance studies of sedimentary rocks. Sedimentary Geology, 182,
651 143–162. <https://doi.org/10.1016/j.sedgeo.2005.07.011>
- 652 Oriolo, S., Schulz, B., Geuna, S., González, P. D., Otamendi, J. E., Sláma, J., Druguet, E.,
653 Siegesmund, S., 2021. Early Paleozoic accretionary orogens along the Western
654 Gondwana margin. Geoscience Frontiers, 12 (1), 109–130.
655 <https://doi.org/10.1016/j.gsf.2020.07.001>
- 656 Pereira, M.F., El Houïcha, M., Aghzer, A., Silva, J.B., Linnemann, U., Jouhari, A., 2014. New
657 U-Pb zircon dating of late Neoproterozoic magmatism in Western Meseta (Morocco).
658 Gondwana 15 - North meets South. 133.
- 659 Pereira, M.F., El Houïcha, M., Chichorro, M., Armstrong, R., Jouhari, A., El Attari, A., Ennih,
660 N., Silva, J.B., 2015. Evidence of a Paleoproterozoic basement in the Moroccan Variscan
661 belt (Rehamna Massif, Western Meseta). Precambrian Research, 268, 61–73.
662 <https://doi.org/10.1016/j.precamres.2015.07.010>
- 663 Pérez-Cáceres, I., Martínez Poyatos, D., Simancas, J.F., Azor, A., 2017. Testing the Avalonian
664 affinity of the South Portuguese Zone and the Neoproterozoic evolution of SW Iberia
665 through detrital zircon populations. Gondwana Research, 42, 177–192.
666 <https://doi.org/10.1016/j.gr.2016.10.010>
- 667 Perez, N.D., Teixell, A., Gómez-Gras, D., Stockli, D.F., 2019. Reconstructing Extensional
668 Basin Architecture and Provenance in the Marrakech High Atlas of Morocco:
669 Implications for Rift Basins and Inversion Tectonics. Tectonics, 38, 1584–1608.
670 <https://doi.org/10.1029/2018TC005413>
- 671 Piqué, A., Jeannette, D., Michard, A., 1980. The Western Meseta Shear Zone, a major and
672 permanent feature of the Hercynian belt of Morocco. Journal of Structural Geology, 2(1–
673 2), 55–61. [https://doi.org/10.1016/0191-8141\(80\)90034-6](https://doi.org/10.1016/0191-8141(80)90034-6)
- 674 Piqué, A., Bossière, G., Bouillin, J.-P., Chalouan, A., Hoepffner, C., 1993a. Southern margin
675 of the Variscan belt: the north-western Gondwana mobile zone (eastern Morocco and
676 Northern Algeria). Geologische Rundschau, 82, 432–439.
677 <https://doi.org/10.1007/BF00212407>
- 678 Piqué, A., El Hassani, A., Hoepffner C., 1993b. Les déformations ordoviciennes dans la zone
679 des Sehoul (Maroc septentrional) : une orogénèse calédonienne en Afrique du Nord.
680 Canadian Journal of Earth Sciences, 30(7), 1332–1337. <https://doi.org/10.1139/e93-114>
- 681 Razin, P., Baudin, T., Chèvremont, P., Andries, D., Youbi, N.A., Hoepffner, C., Thiéblemont,
682 D., Chihani, E.M., 2003. Carte géologique du Maroc au 1/50 000, feuille de Jebel
683 Kharrou, Mémoire explicatif. Notes et Mémoires du Service Géologique du Maroc, Rabat
684 436 bis, 1–105.
- 685 Reiners, P.W., Carlson, R.W., Renne, P.R., Cooper, K.M., Granger, D.E., McLean, N.M.,
686 Schoene, B., 2017. Geochronology and thermochronology, John Wiley & Sons Ltd, 1–
687 464. <https://doi.org/10.1002/9781118455876>

- 688 Ribeiro, A., Munhá, J., Dias, R., Mateus, A., Pereira, E., Ribeiro, L., Fonseca, P., Araújo, A.,
689 Oliveira, T., Romão, J., Chaminé, H., Coke, C., Pedro, J., 2007. Geodynamic evolution
690 of the SW Europe Variscides. *Tectonics*, 26, TC6009.
691 <https://doi.org/10.1029/2006TC002058>
- 692 Rubatto, D. 2002. Zircon trace element geochemistry: Partitioning with garnet and the link
693 between U–Pb ages and metamorphism. *Chemical Geology*, 184, 123–138.
694 [https://doi.org/10.1016/S0009-2541\(01\)00355-2](https://doi.org/10.1016/S0009-2541(01)00355-2)
- 695 Simancas, J.F., Tahiri, A., Azor, A., Lodeiro, F.G., Poyatos, D.J.M., 2005. The tectonic frame
696 of the Variscan–Alleghanian orogen in Southern Europe and Northern Africa.
697 *Tectonophysics*, 398, 181–198. <https://doi.org/10.1016/j.tecto.2005.02.006>
- 698 Simancas, J.F., Azor, A., Martínez-Poyatos, D., Tahiri, A., El Hadi, H., González-Lodeiro, F.,
699 Pérez-Estaún, A., Carbonell, R., 2009. Tectonic relationships of Southwest Iberia with
700 the allochthons of Northwest Iberia and the Moroccan Variscides. *Comptes Rendus*
701 *Geoscience*, 341, 103–113. <http://dx.doi.org/10.1016/j.crte.2008.11.003>
- 702 Sláma, J., Kosler, J., Condon, D.J., Crowley, J.L., Gerdes, A., Hanchar, J.M., Horstwood,
703 M.S.A., Morris, G.A., Nasdala, L., Norberg, N., Schaltegger, U., Schoene, B., Tubrett,
704 M.N., Whitehouse, M.J., 2008. Plesovice zircon - A new natural reference material for
705 U–Pb and Hf isotopic microanalysis. *Chemical Geology*, 249, 1–35.
706 <https://doi.org/10.1016/j.chemgeo.2007.11.005>
- 707 Spencer, C.J., Kirkland, C.L., Taylor, R.J.M., 2016. Strategies towards statistically robust
708 interpretations of in situ U–Pb zircon geochronology. *Geoscience Frontiers*, 7, 581–589.
709 <https://doi.org/10.1016/j.gsf.2015.11.006>
- 710 Stampfli, G.M., Borel, G.D., 2002. A plate tectonic model for the Paleozoic and Mesozoic
711 constrained by dynamic plate boundaries and restored synthetic oceanic isochrons. *Earth*
712 *and Planetary Science Letters*, 196, 17–33. [https://doi.org/10.1016/S0012-821X\(01\)00588-X](https://doi.org/10.1016/S0012-821X(01)00588-X)
- 714 Stampfli, G.M., Vavassis, I., De Bono, A., Rosselet, F., Matti, B., Bellini, M., 2003. Remnants
715 of the paleotethys oceanic suture-zone in the western tethyan area. *Bollettino della*
716 *Società Geologica Italiana*, 2, 1–23.
- 717 Stampfli, G.M., Hochard, C., Vêrard, C., Wilhem, C., VonRaumer, J., 2013. The formation of
718 Pangea. *Tectonophysics*, 593, 1–19. <https://doi.org/10.1016/j.tecto.2013.02.037>
- 719 Tahiri, A., Montero, P., El Hadi, H., Martínez Poyatos, D., Azor, A., Bea, F., Simancas, J.F.,
720 González Lodeiro, F., 2010. Geochronological data on the Rabat-Tiflet granitoids: Their
721 bearing on the tectonics of the Moroccan Variscides. *Journal of African Earth Sciences*,
722 57, 1–13. <https://doi.org/10.1016/j.jafrearsci.2009.07.005>
- 723 Thomas, W.A., 2011. Detrital-zircon geochronology and sedimentary provenance. *Lithosphere*,
724 3, 304–308. <https://doi.org/10.1130/RF.L001.1>
- 725 Vermeesch, P., 2004. How many grains are needed for a provenance study? *Earth and Planetary*
726 *Science Letters*, 224, 441–451. <https://doi.org/10.1016/j.epsl.2004.05.037>
- 727 Vermeesch, P., 2018. IsoplotR: A free and open toolbox for geochronology. *Geoscience*
728 *Frontiers*, 9, 1479–1493. <https://doi.org/10.1016/j.gsf.2018.04.001>
- 729 Wernert, P., Schulmann, K., Chopin, F., Štípská, P., Bosch, D., El Houicha, M., 2016.
730 Tectonometamorphic evolution of an intracontinental orogeny inferred from P–T–t–d
731 paths of the metapelites from the Rehamna massif (Morocco). *Journal of Metamorphic*
732 *Geology*, 34, 917–940. <https://doi.org/10.1111/jmg.12214>
- 733 Wiedenbeck, M., Allé, P., Corfu, F., Griffin, W.L., Meier, M., Oberli, F., Von Quadt, A.,
734 Roddick, J.C., Spiegel, W., 1995. Three natural zircon standards for U–Th–Pb, Lu–Hf,
735 trace element and REE analyses. *Geostandards Newsletter*, 19, 1–23.
736 <https://doi.org/10.1111/j.1751-908X.1995.tb00147.x>

737 Zimmermann, S., Mark, C., Chew, D., Voice, P.J., 2018. Maximising data and precision from
738 detrital zircon U-Pb analysis by LA-ICPMS: The use of core-rim ages and the single-
739 analysis concordia age. *Sedimentary Geology*, 375, 5–13.
740 <https://doi.org/10.1016/j.sedgeo.2017.12.020>

741 **Figure Caption**

742 **Fig. 1.** Simplified geological map of the Moroccan Variscides (modified after Hoepffner *et al.*,
743 2005; Michard *et al.*, 2010 in Chopin *et al.*, 2014). Middle Meseta Fault Zone (MMFZ),
744 Western Meseta Shear Zone (WMSZ), South Meseta Fault (SMF), South Meseta Front (SMFr),
745 South Atlas Fault (SAF), Rabat-Tiflet Fault Zone (RTFZ), Sidi Bettache Basin (SBB), and
746 Azrou-Khenifra Basin (AKB).

747 **Fig. 2.** Simplified Geological map of the Rehamna massif (adapted from Corsini, 1988; Baudin
748 *et al.*, 2003; Chopin *et al.*, 2014; Pereira *et al.*, 2015; El Houicha *et al.*, 2018).

749 **Fig. 3.** Synthetic lithostratigraphic logs of the Rehamna massif subdivided into the Western
750 (i.e., Coastal Block), Central and Eastern Rehamna, and the lower and upper metamorphic units
751 (modified after Michard, 1982; Hoepffner, 1974; Corsini *et al.*, 1988; Baudin *et al.*, 2003;
752 Chopin *et al.*, 2014; Pereira *et al.*, 2015; El Houicha *et al.*, 2018).

753 **Fig. 4.** Field photographs of the sample location. (a) A quarry at the southwest of the Sebt
754 Brikyine granite showing the Paleoproterozoic basement and its early Cambrian sedimentary
755 cover (modified after Pereira *et al.*, 2015); (b) Basal early Cambrian microbreccia/(meta)arkose
756 (R161-A); (c) Panorama of a quartzitic layer from the Skhour Formation at Koudiat Karkaba
757 (SK1-Z); (d) Cross section and (e) field photograph of the Ouled Zednes Fault Zone (modified
758 after Jenny, 1974) with location of the sample R255-OZ and location of the Eifelian-Frasnian
759 corals from El Houicha *et al.* (2019); (f) Sandstone (R255-OZ); (g) Quartzite from the Ouled
760 Hassine-Ouled Zednes Formation at Souq el Had (R257-OH); (h) Dalaat Formation; (i) Detail
761 of the Dalaat Formation showing layered (calcareous)sandstone (R256-DT).

762 **Fig. 5. (a-e)** Microphotographs of the samples R16-1A, SK1-Z, R255-OZ, R257-OH and R256-
763 DT. Mineral abbreviations: Qtz: quartz, Ms: white micas, Cal: calcite.

764 **Fig. 6.** Cathodoluminescence images of selected zircon grains.

765 **Fig. 7.** (a) Concordia diagrams of the sample R16-1A. Green circles (concordant); Gray circles
766 (discordant); (b) Zircon U–Pb Kernel Density Estimator (KDE) diagrams for the sample R16-
767 1A. Red dots indicate Th/U ratios.

768 **Fig. 8.** (a) Concordia diagrams, zircon U–Pb Kernel Density Estimation (KDE) diagrams and
769 percentage of different population age groups for the samples (a) SK1-Z, (b) R257-OH, (c)
770 R255-OZ and (d) R256-DT. Red circles (concordant); Gray circles (discordant).

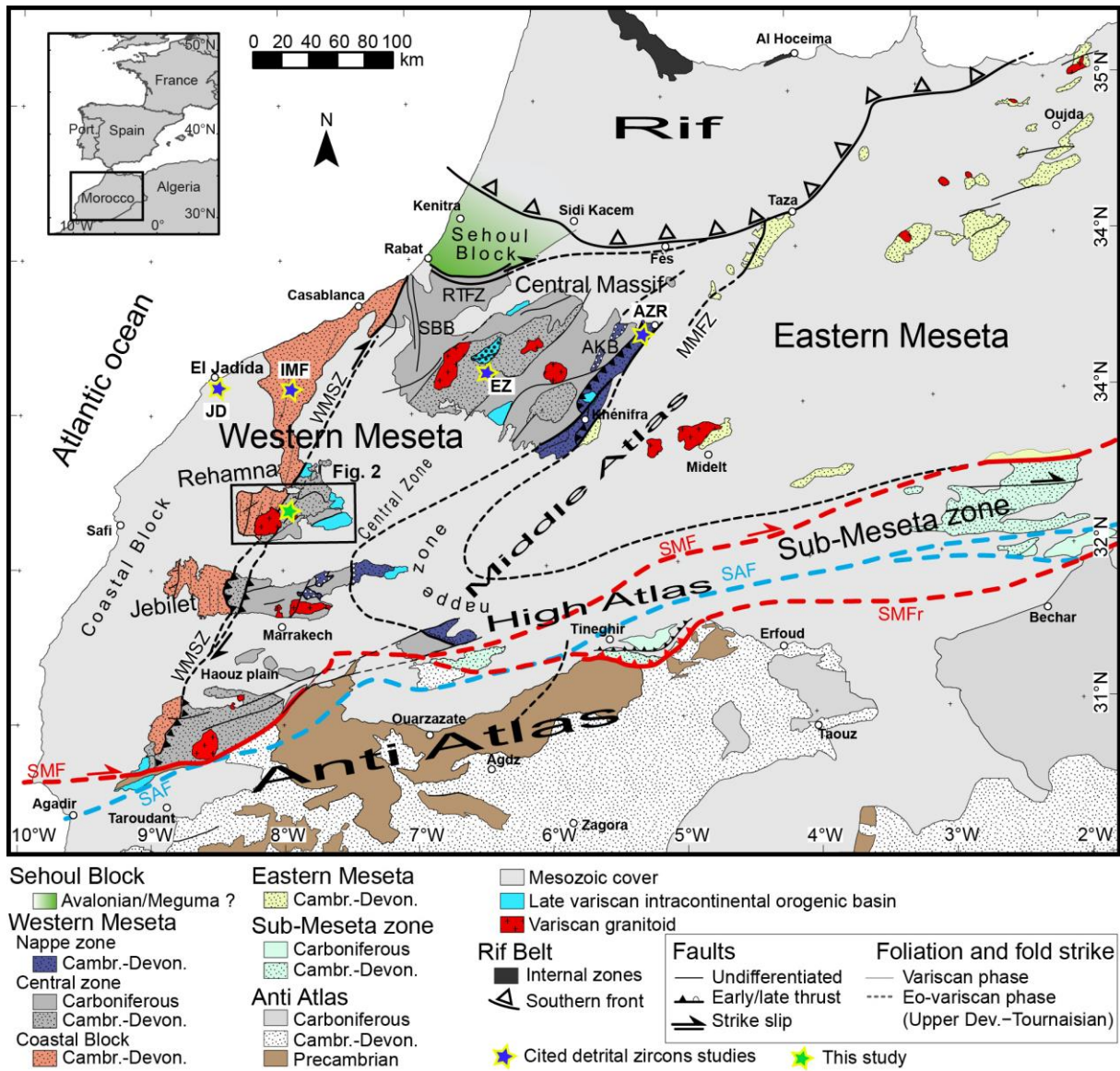
771 **Fig. 9.** Conceptual tectonic and sediment dispersal evolution of the Rehamna massif during the
772 (a) early Cambrian (see El Houicha *et al.*, 2018 for more details), (b) Ordovician, (c) Devonian
773 and (d) early Carboniferous (coeval tectonic structures are omitted). Black arrows represent
774 sourcing properly identified in our zircon age spectra, while grey arrows represent hypothesized
775 and later remobilized sourcing only found in younger zircon age spectra.

776 **Fig. 10.** Paleogeographic reconstruction (modified after Martinez Catalan *et al.*, 2021) showing
777 probable Ordovician to early Carboniferous sources for clastic sediments sampled in the
778 Rehamna massif.

779 **Table 1.** List of samples with details of the analyses carried out on the zircon grains.

780

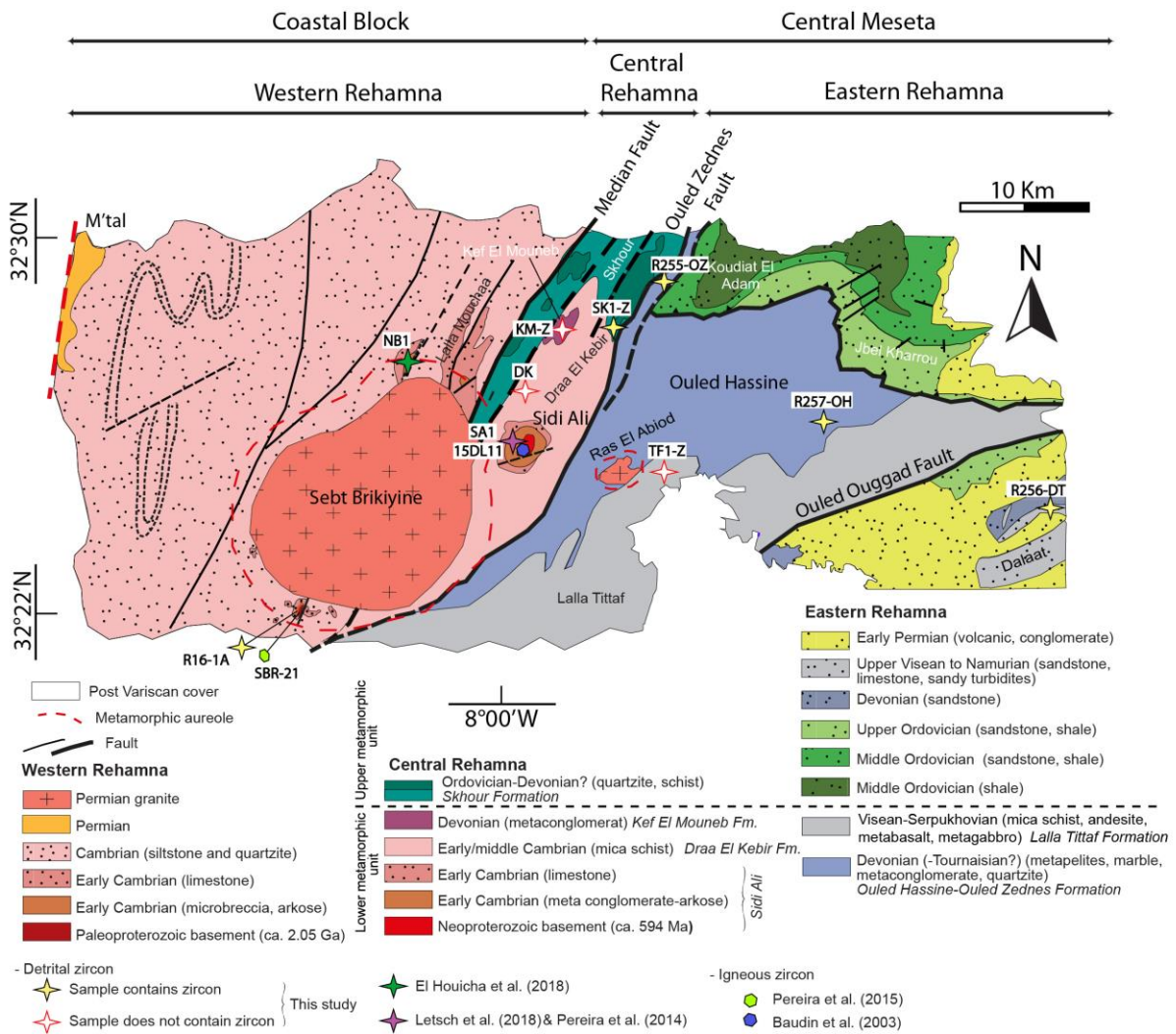
781 **Fig. 1.**



782

783

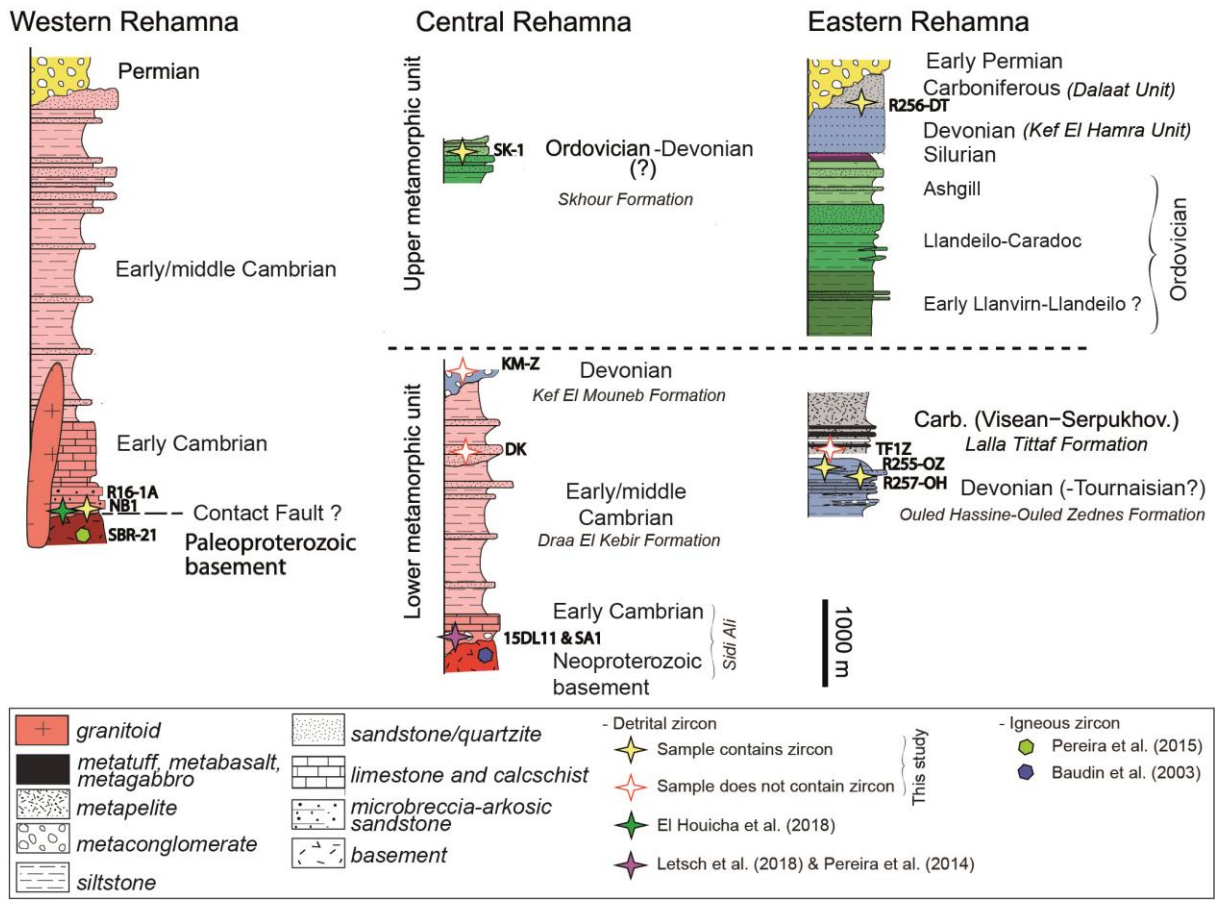
784 **Fig. 2.**



785

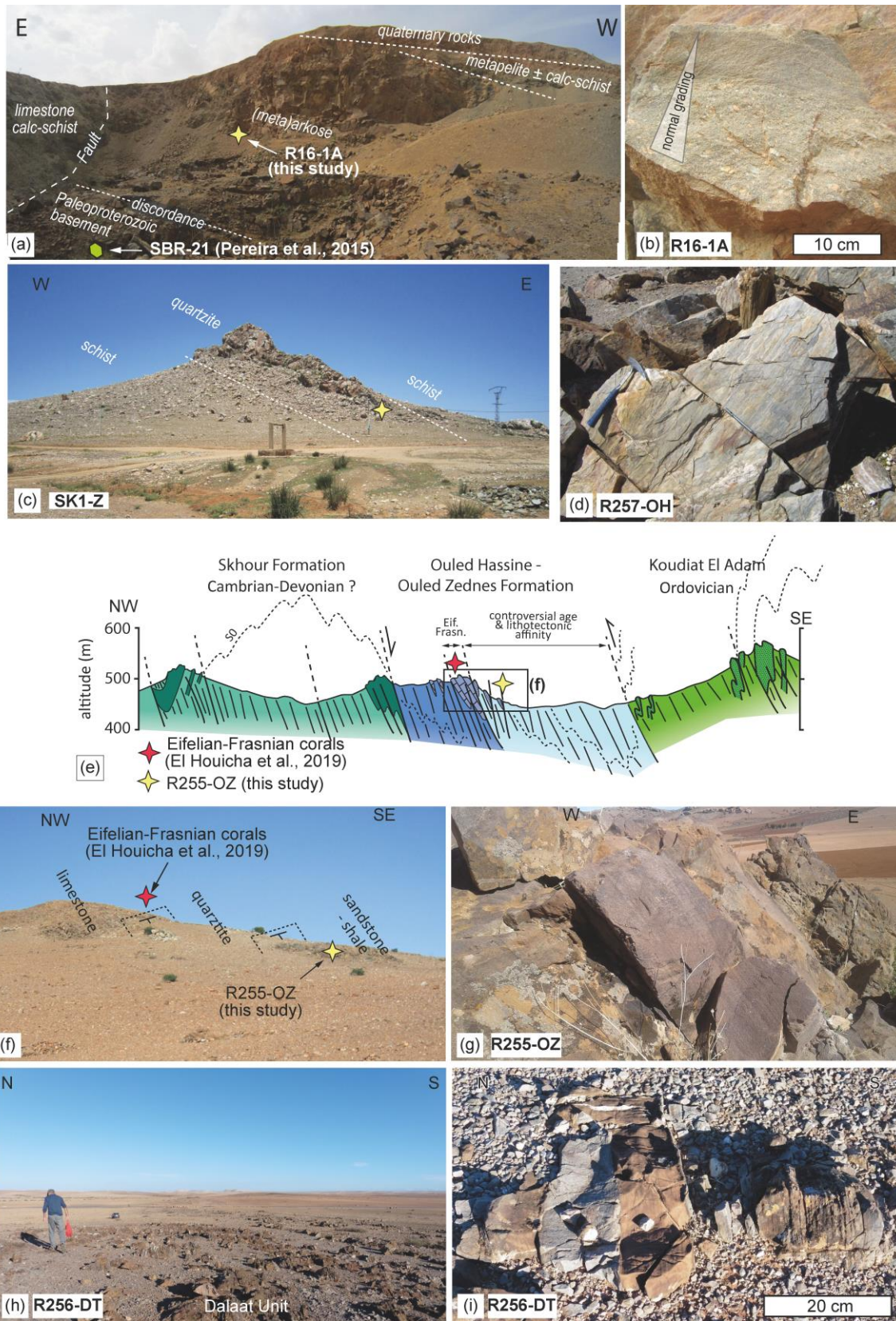
786

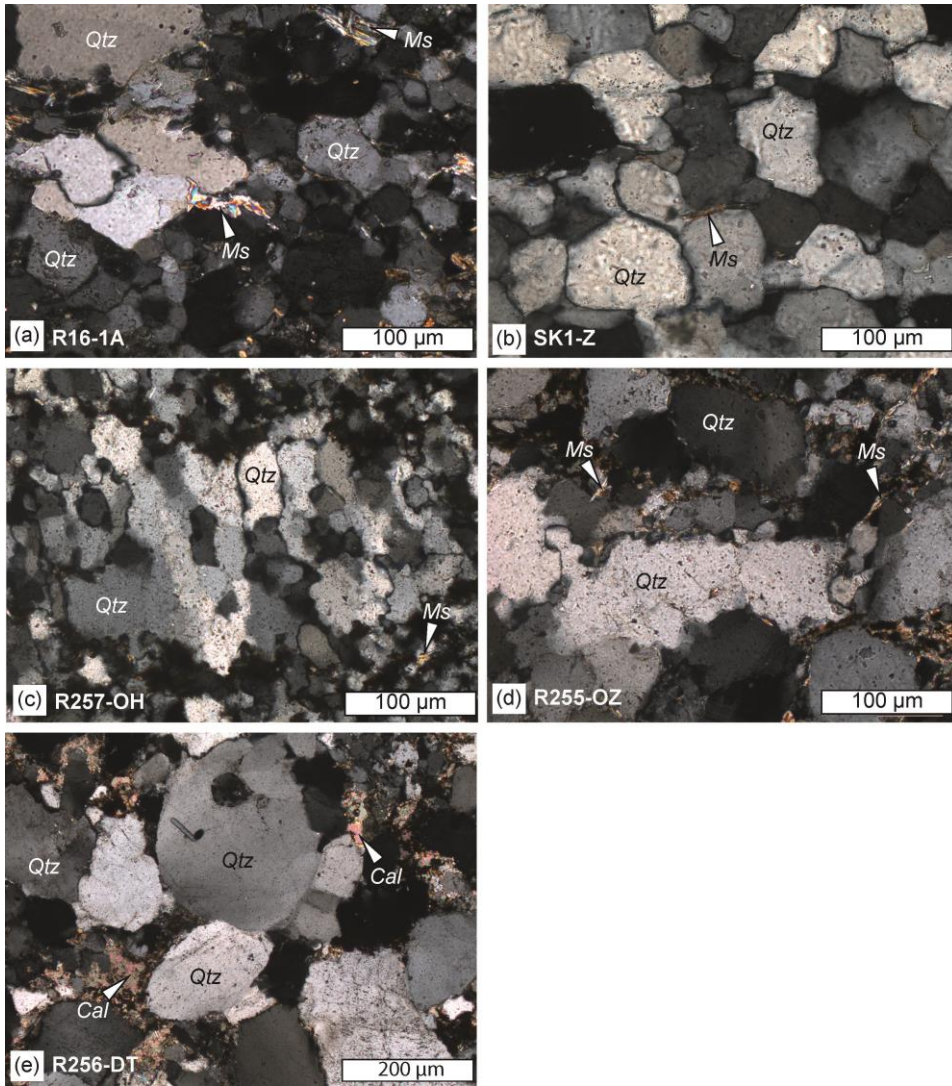
787 **Fig. 3.**

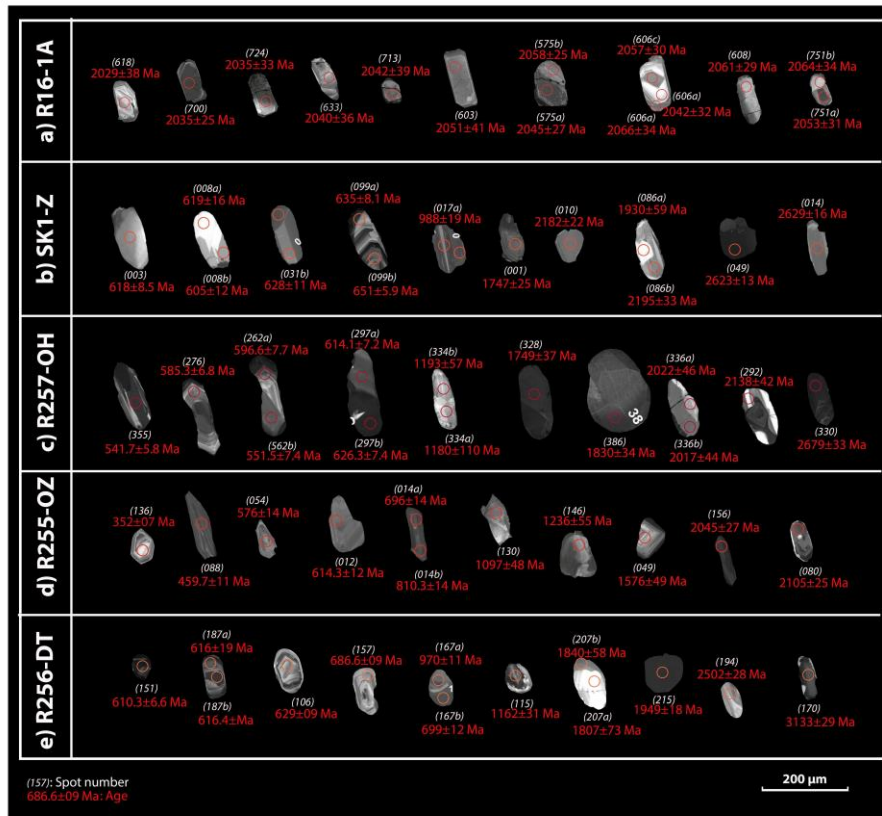


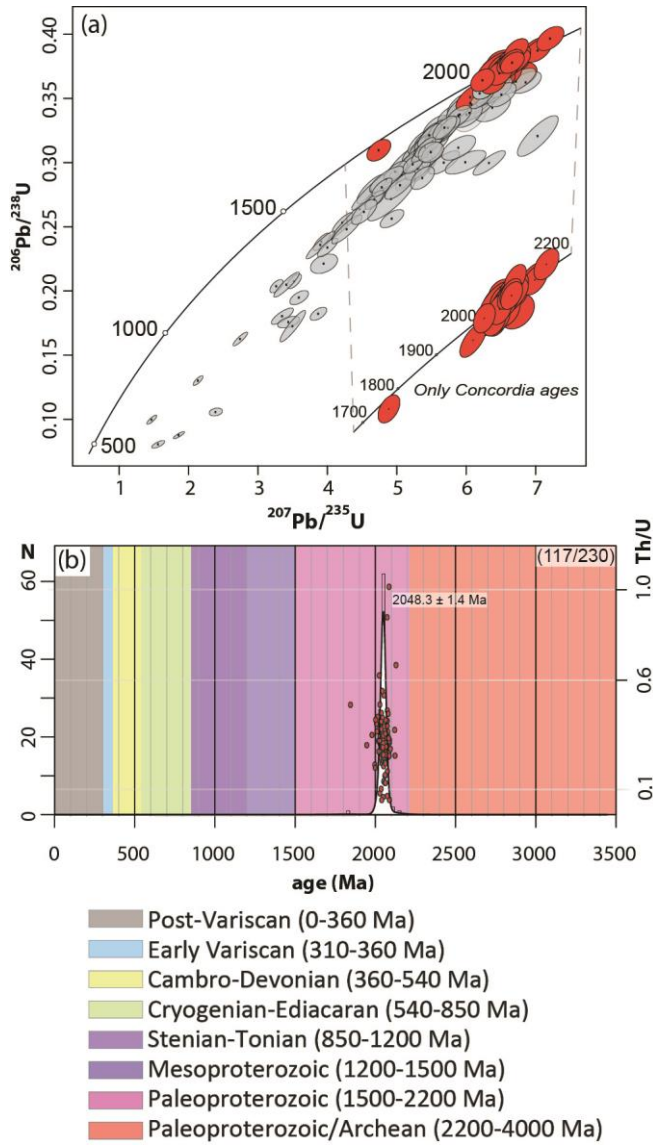
788

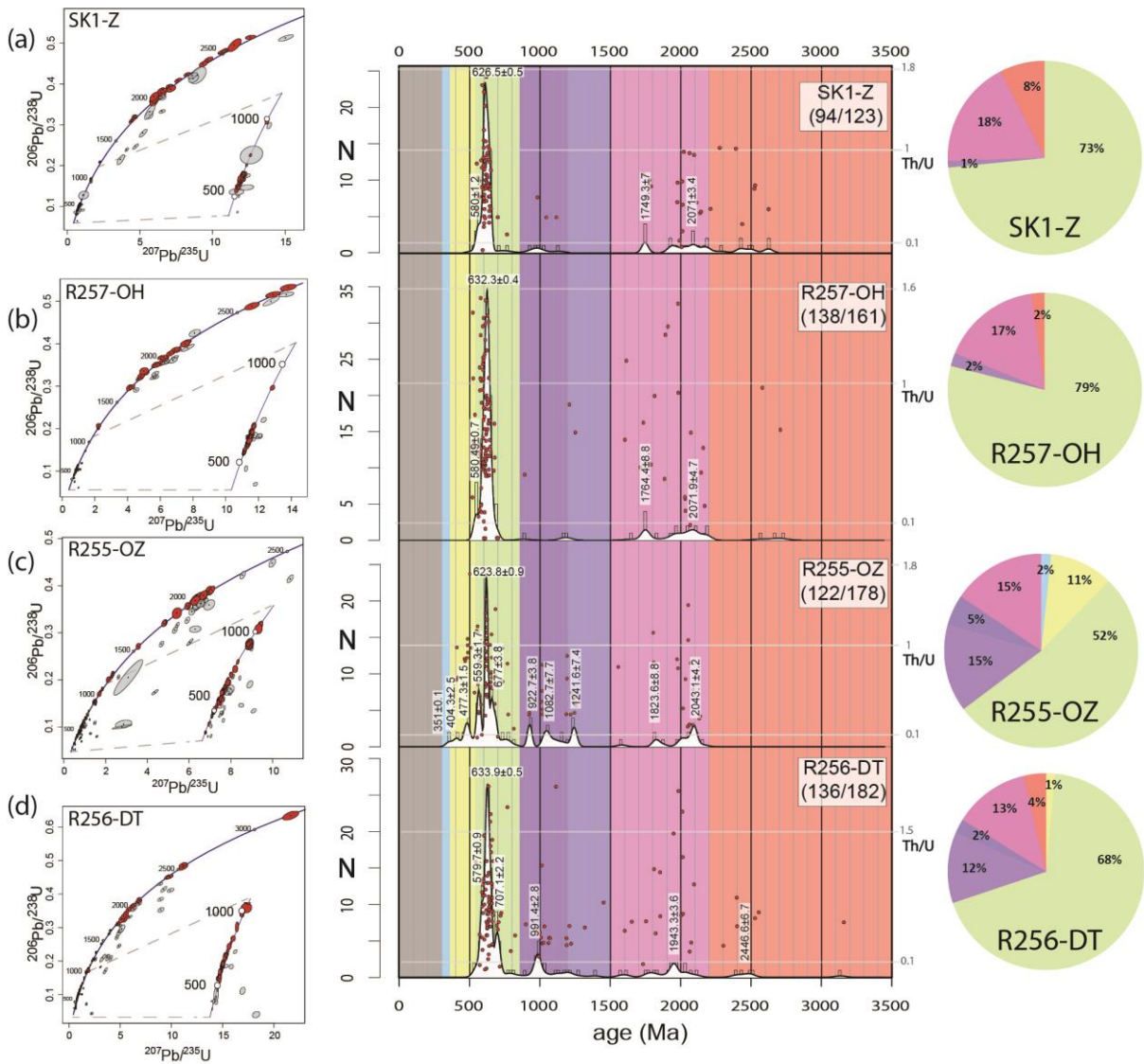
789



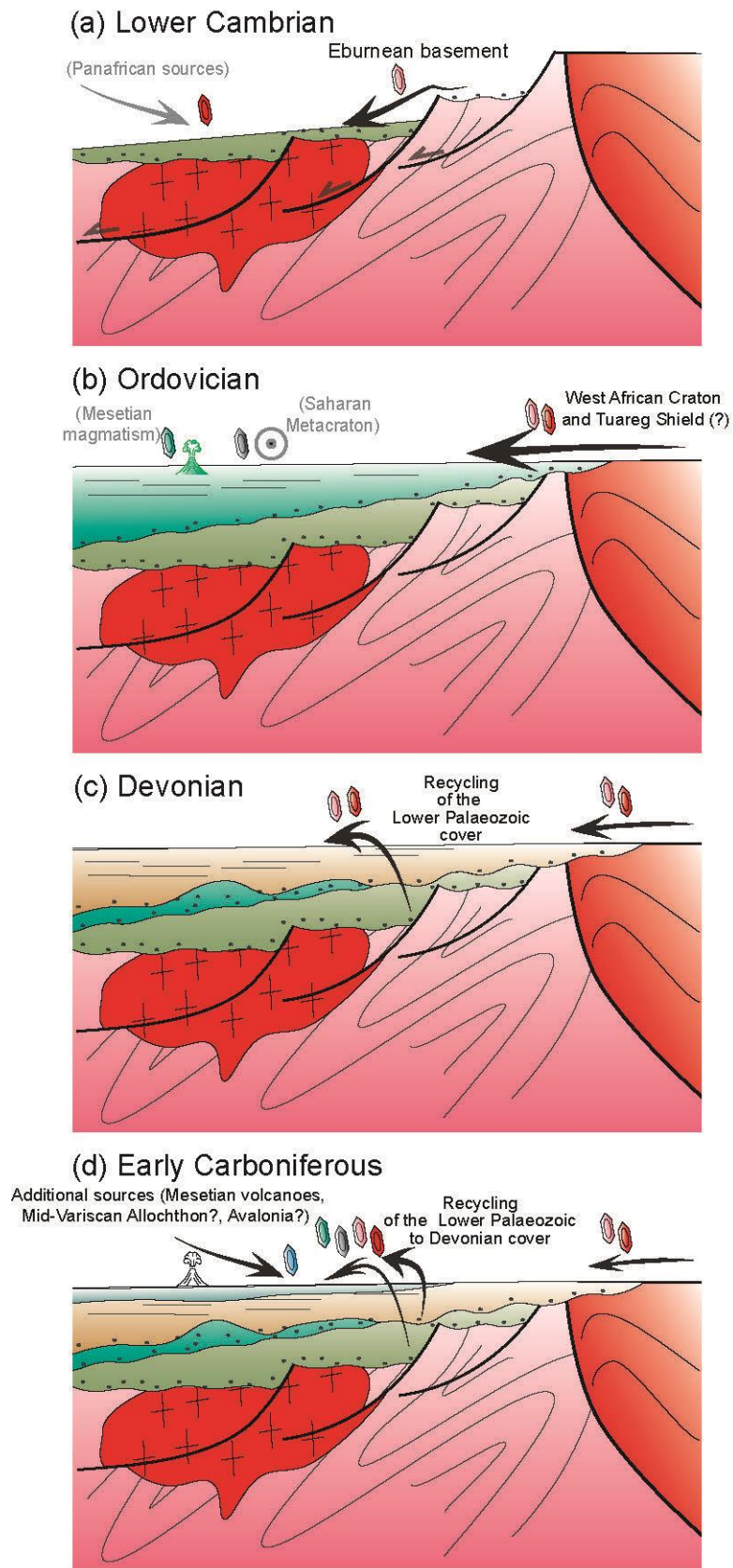


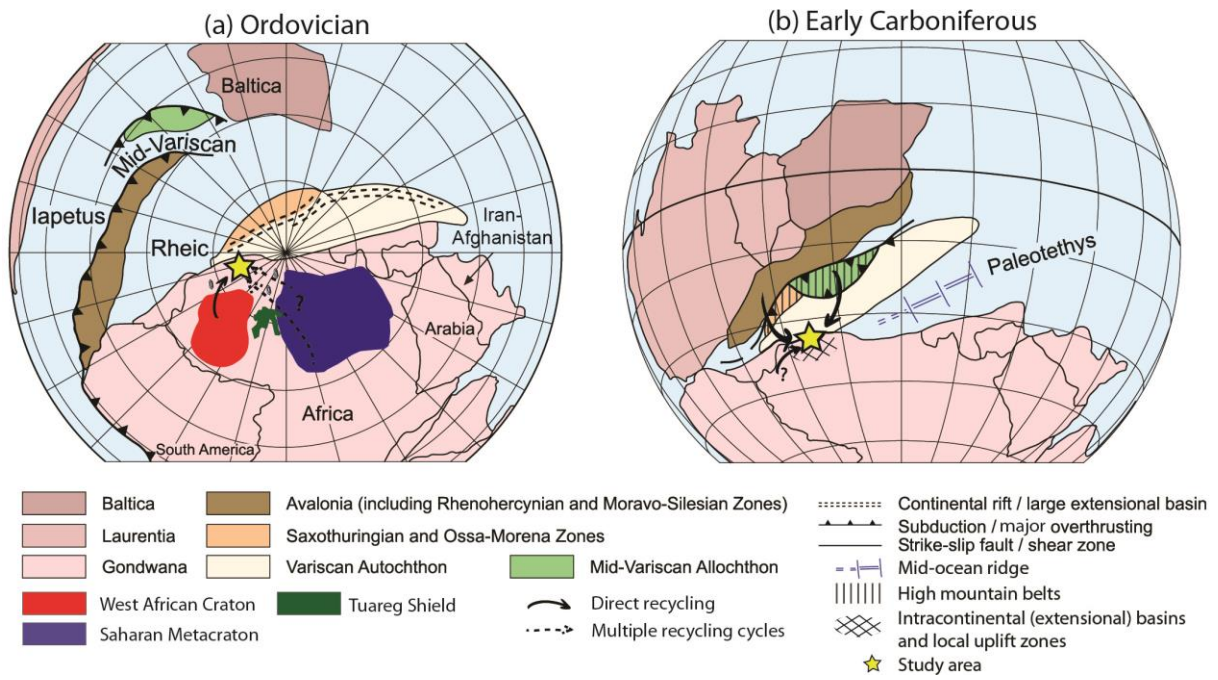






799
800





Block/Unit/Formation	Site	Sample	Long.	Lat.	Lithostratigraphy (from literature)	Sample's age (this study)	Lithology	Zircon grains analyzed	Number of concordant analyses/ Number of analyses
Dahaat unit	Dahaat formation	R256-DL	-7.523870	32.337190	Middle (?)-late Viséan (Razin et al., 2003)	idem	sandstone	175	136/182
Ouled Hassine-Ouled Zednes	Jaufa	R257-OH	-7.730770	32.373330	Lower or Middle to Upper Devonian (e.g. Hoepfner 1974; Comé, 1982; Razin et al., 2003)	idem	quartzitic lense	173	138/161
Lalla Titaf	Imi	TF1Z	-7.865546	32.336293	Carboniferous (?) (Hoepfner et al., 1974)	idem	quartzite interlayered in mica schist	no zircon	no zircon
Ouled Hassine-Ouled Zednes	Ouled Zednes Fault Zone	R255-OZ	-7.850210	32.484050	Upper Devonian (post-Frasnian) to Dinantian (Jenny, 1974; Baudin et al., 2002; Razin 2003)	Tournaisian (maximum depositional age)	quartzitic lense	292	122/178
Kef El Mouneh	Kef El Mouneh	KM-Z	-7.949580	32.427268	Cambro-Ordovician or Upper Devonian (Boudin et al., 2003; Razin, 2003)	idem	coarse meta-conglomerate	no zircon	no zircon
Skhour	Koulat Karleba	SK1-Z	-7.898843	32.439914	Devonian (?) (Destombes et al., 1982; Baudin et al., 2003)	Ordovician	quartzite	99	94/123
Draa el Kehir	Draa el Kehir	DK	-7.986895	32.386054	Ordovician-Devonian (?) (Baudin et al., 2003)	idem	quartzite interlayered in mica schist	no zircon	no zircon
Coastal block	SW of the Sebti Brilkyine granite	R16-1A	-8.172580	32.226670	Middle Cambrian (?) (Corsini et al., 1988)	idem	arkose-sandstone	196	117/230